ARMY RESEARCH LABORATORY

Two Projectiles Connected by a Flexible Tether Dropped in the Atmosphere

by Geoffrey W. Frost
and Mark F. Costello

ARL-CR-453 July 2000

The findings in this report are not to be construed as an official Department of the Army position unless so designated by other authorized documents.

Citation of manufacturer's or trade names does not constitute an official endorsement or approval of the use thereof.

Destroy this report when it is no longer needed. Do not return it to the originator.

Army Research Laboratory
Aberdeen Proving Ground, MD 21005-5066

ARL-CR-453 **July 2000**

Two Projectiles Connected by a Flexible Tether Dropped in the Atmosphere

Geoffrey W. Frost and Mark F. Costello
Oregon State University

Abstract

This study investigates the atmospheric flight dynamics of a munition system that is released from an aircraft at altitude and drops toward a target on the ground. The munition system consists of two projectiles connected by a tether line. Initially, the two projectiles are rigidly attached. At a specified time, the projectiles separate and subsequently unreel the tether line. After the tether line is fully payed out, the system settles toward a steady state as it approaches the ground. It is shown that while projectile position results converge for a relatively low number of tether line elements, the maximum tether loads require a significantly larger number of elements. For a low follower-to-lead projectile mass ratio, the tether line unreeling process is predominantly due to the follower and lead projectile separation. Conversely, for a high follower-to-lead projectile mass ratio, the tether line tends to billow and subsequently unreel itself, independent of the lead and follower projectile motion.

Table of Contents

		Page
	List of Figures	v
	List of Tables	vii
1.	Introduction	1
2.	Dynamic Model for a Fully Deployed Tether	1
3.	Tether Line Deployment Model	8
4.	Simulation Results	9
5.	Effect of Projectile Drag Coefficient Ratio for a Low Mass Ratio Configuration	13
6.	Effect of Projectile Drag Coefficient Ratio for a High Mass Ratio Configuration	18
7.	Effect of Tether Stiffness for a Low Mass Ratio Configuration	25
8.	Conclusions	29
9.	References	31
	List of Symbols	33
	Distribution List	35
	Report Documentation Page	41

INTENTIONALLY LEFT BLANK.

List of Figures

Figure		Page
1.	Flight Phases for the Weapons Systems Concept	2
2.	Model Diagram and Inertial Reference Frame	3
3.	Aerodynamic Velocities Diagram	7
4.	Maximum Position Error of Follower	11
5.	Maximum Line Load	12
6.	Total Number of Time Steps	13
7.	Number of Steps vs. Time for the Pop-Out Method	14
8.	Number of Steps vs. Time for the All-Out Method	14
9.	Range of Lead and Follower (Lead/Follower Mass Ratio 1%)	15
10.	Lineout (Lead/Follower Mass Ratio 1%)	16
11.	Pop-Out Method Tether Shape Sequence (Mass Ratio 1%; Drag Ratio 2/1)	17
12.	Speed of Lead Projectile (Lead/Follower Mass Ratio 1%)	19
13.	Speed of Follower Projectile (Lead/Follower Mass Ratio 1%)	19
14.	Maximum Line Load (Lead/Follower Mass Ratio 1%; 100 Beads)	20
15.	Maximum Acceleration of Follower (Lead/Follower Mass Ratio 1%; 100 Beads)	20
16.	Range of Lead and Follower (Lead/Follower Mass Ratio 100%)	21
17.	Lineout (Lead/Follower Mass Ratio 100%)	22
18.	Pop-Out Method Tether Shape Sequence (Mass Ratio 100%; Drag Ratio 2/1)	23
19.	Speed of Lead Projectile (Pop-Out Method - Lead/Follower Mass Ratio 100%)	24
20.	Speed of Follower Projectile (Pop-Out Method – Lead/Follower Mass Ratio 100%)	25

Figure		Page
21.	Range of Lead and Follower (Lead/Follower Mass Ratio 1%)	26
22.	Lineout (Lead/Follower Mass Ratio 1%)	27
23.	Speed of Lead Projectile (Lead/Follower Mass Ratio 1%)	27
24.	Speed of Follower Projectile (Lead/Follower Mass Ratio 1%)	28
25.	Maximum Line Load (Lead/Follower Mass Ratio 1%; 100 Beads)	28
26.	Maximum Acceleration of Follower (Lead/Follower Mass Ratio 1%; 100 Beads)	29

List of Tables

Table		Page
1.	Nominal Simulation Values	10

INTENTIONALLY LEFT BLANK.

1. Introduction

Connecting two bodies by means of a tether has been utilized in many aerospace applications including tethered spacecraft [1, 2], aircraft air refueling [3, 4], and atmospheric balloons [5]. More recently, designers have concepted weapon systems with two projectiles connected by a tether line [6]. In these concepts, the lead projectile is generally a munition and the follower projectile is a sensor platform. The scenario investigated here assumes the weapon is released from an aircraft at altitude and drops to a target. Initially, both projectiles are rigidly attached. The projectiles separate and at a prespecified time the tether line begins to unreel. When the tether line is completely payed out, the system approaches a steady-state as the projectiles and tether line approach the target. A schematic of the various flight phases for the weapon system concept is shown in Figure 1. The work presented here first develops a flight dynamic model suitable for simulating the event described. This model is subsequently exercised to investigate how primary system design parameters such as projectile mass ratio, drag coefficient ratio, and tether stiffness effect overall performance of the weapon.

2. Dynamic Model for a Fully Deployed Tether

As previously mentioned, the actual weapon system consists of two projectiles connected by a flexible tether. This is modeled as a series of nodes or beads connected by springs and dampers arranged in parallel, as depicted in Figure 2. The lead and follower projectiles are assumed to be stable and are modeled as point masses with three translational degrees of freedom. Likewise, each tether bead is modeled as a point mass, also with three translational degrees of freedom. Both projectiles and the tether beads are acted upon by gravitational, aerodynamic, and elastic forces. The lead and follower objects are designated as the 0 and n nodes, respectively. The tether is split into n—1 point mass beads are designated by j, and n line elements are designated with i. The earth's surface is used as an inertial reference frame. Air density is computed using a standard atmosphere model [7].

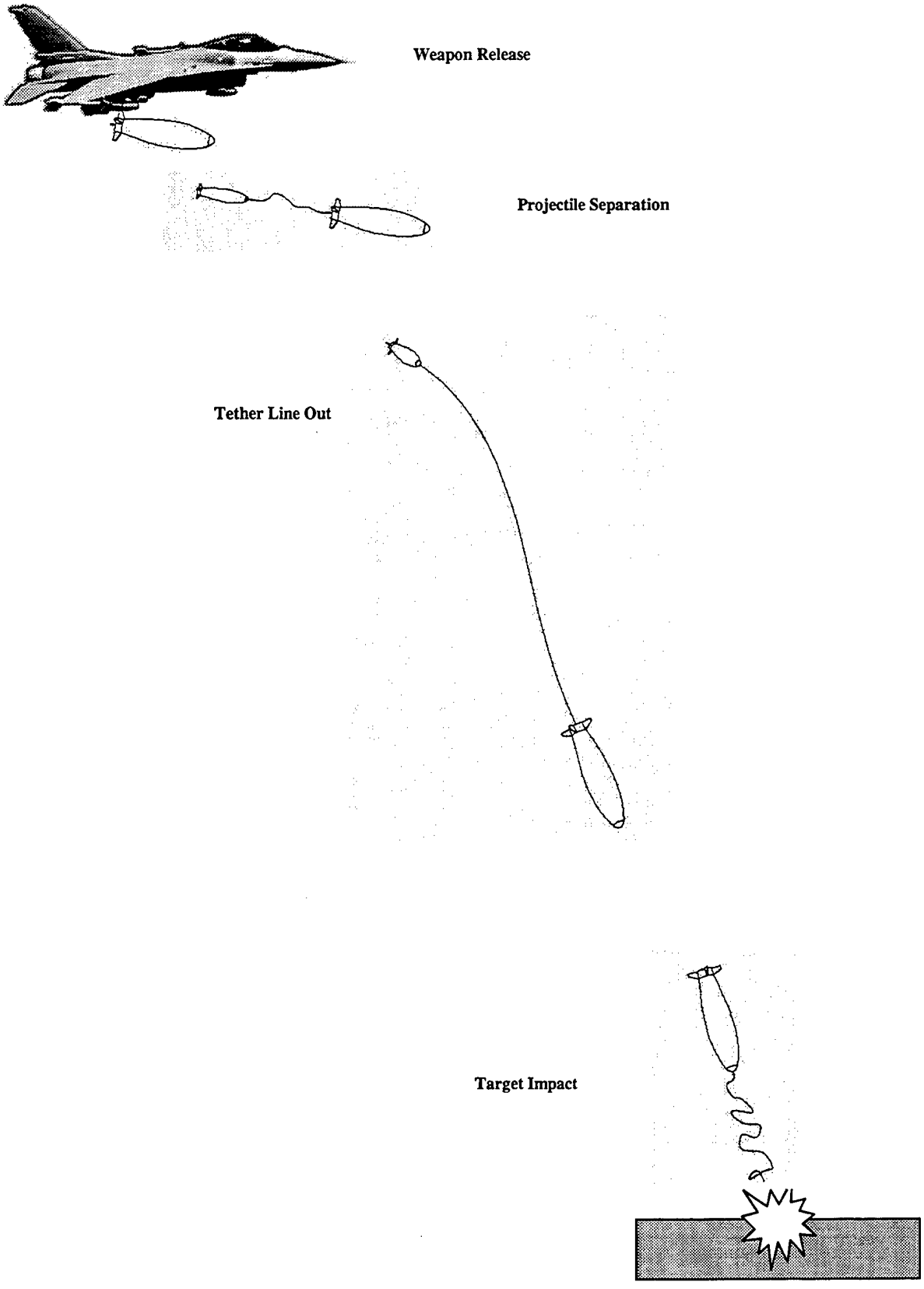

Figure 1. Flight Phases for the Weapons Systems Concept.

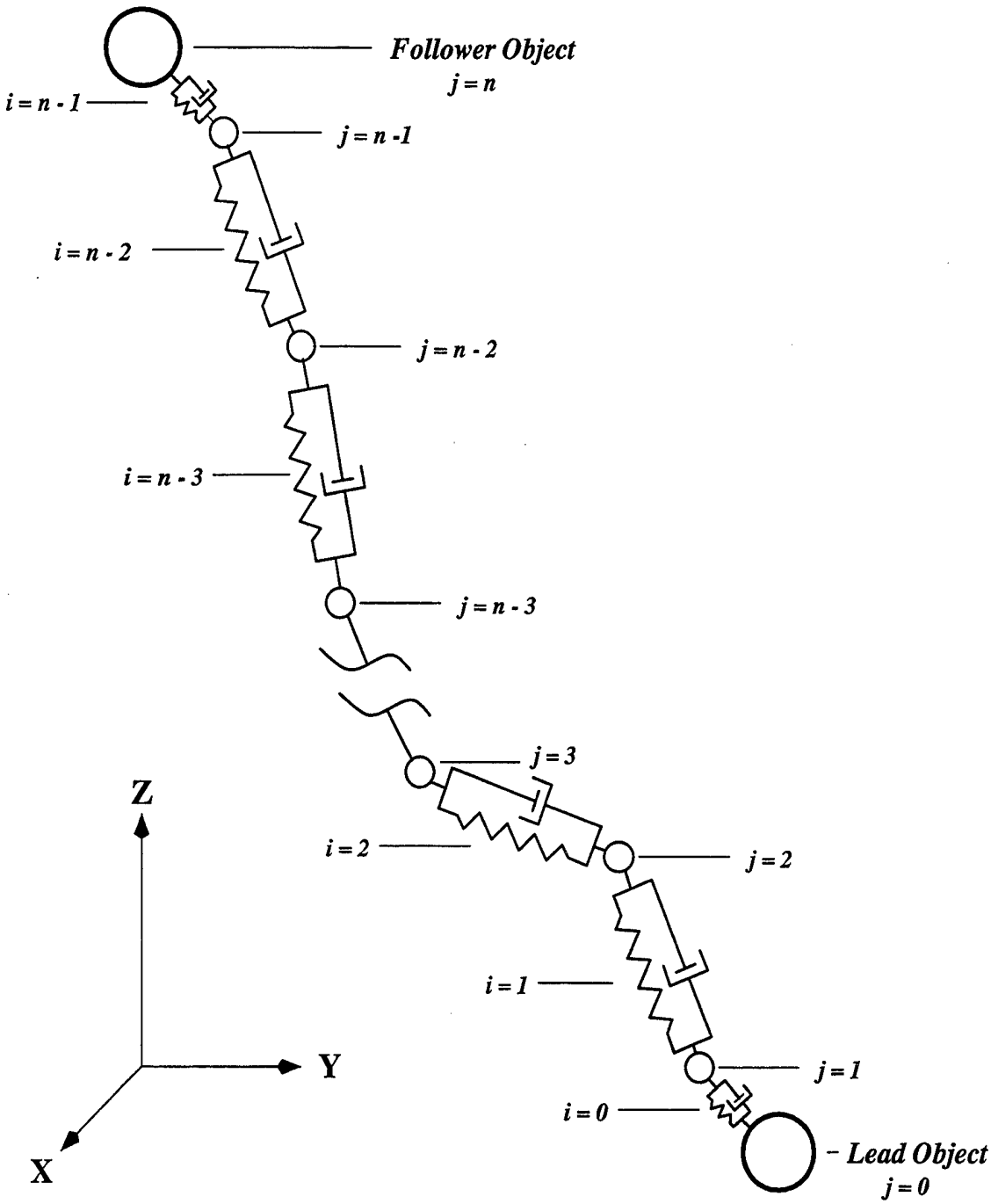

Figure 2. Model Diagram and Inertial Reference Frame.

When the tether is fully deployed, the equations of motion for the follower projectile (n) and the *jth* tether bead are given in equations 1 and 2.

$$m_n \begin{Bmatrix} \ddot{x} \\ \ddot{y} \\ \ddot{z} \end{Bmatrix}_n = \begin{Bmatrix} X_A \\ Y_A \\ Z_A \end{Bmatrix}_n - \begin{Bmatrix} X_T \\ Y_T \\ Z_T \end{Bmatrix}_{n-1} + \begin{Bmatrix} 0 \\ 0 \\ W \end{Bmatrix}_n . \tag{1}$$

$$m_j \begin{Bmatrix} \ddot{x} \\ \ddot{y} \\ \ddot{z} \end{Bmatrix}_j = \begin{Bmatrix} X_T \\ Y_T \\ Z_T \end{Bmatrix}_{i+1} - \begin{Bmatrix} X_T \\ Y_T \\ Z_T \end{Bmatrix}_i + \begin{Bmatrix} X_D \\ Y_D \\ Z_D \end{Bmatrix}_j + \begin{Bmatrix} 0 \\ 0 \\ W_T \end{Bmatrix}_j . \tag{2}$$

The lead projectile (0) equations are identical in form to equation 1. The elastic forces are due to the spring and damping characteristics of the tether. These forces are always parallel to the direction of the line. In order to express the tether-bead-applied loads concisely, the position and velocity matrices shown in equations 3–6 prove useful.

$$\begin{bmatrix} \Delta x_0 & \Delta y_0 & \Delta z_0 \\ \Delta x_1 & \Delta y_1 & \Delta z_1 \\ \vdots & \vdots & \vdots \\ \Delta x_{n-1} & \Delta y_{n-1} & \Delta z_{n-1} \end{bmatrix} = \begin{bmatrix} x_1 - x_0 & y_1 - y_0 & z_1 - z_0 \\ x_2 - x_1 & y_2 - y_1 & z_2 - z_1 \\ \vdots & \vdots & \vdots \\ x_n - x_{n-1} & y_n - y_{n-1} & z_n - z_{n-1} \end{bmatrix} . \tag{3}$$

$$\begin{bmatrix} \Delta \dot{x}_0 & \Delta \dot{y}_0 & \Delta \dot{z}_0 \\ \Delta \dot{x}_1 & \Delta \dot{y}_1 & \Delta \dot{z}_1 \\ \vdots & \vdots & \vdots \\ \Delta \dot{x}_{n-1} & \Delta \dot{y}_{n-1} & \Delta \dot{z}_{n-1} \end{bmatrix} = \begin{bmatrix} \dot{x}_1 - \dot{x}_0 & \dot{y}_1 - \dot{y}_0 & \dot{z}_1 - \dot{z}_0 \\ \dot{x}_2 - \dot{x}_1 & \dot{y}_2 - \dot{y}_1 & \dot{z}_2 - \dot{z}_1 \\ \vdots & \vdots & \vdots \\ \dot{x}_n - \dot{x}_{n-1} & \dot{y}_n - \dot{y}_{n-1} & \dot{z}_n - \dot{z}_{n-1} \end{bmatrix} . \tag{4}$$

$$\begin{bmatrix} \Delta l_0 \\ \Delta l_1 \\ \vdots \\ \Delta l_{n-1} \end{bmatrix} = \begin{bmatrix} \sqrt{\Delta x_0^2 + \Delta y_0^2 + \Delta z_0^2} \\ \sqrt{\Delta x_1^2 + \Delta y_1^2 + \Delta z_1^2} \\ \vdots \\ \sqrt{\Delta x_{n-1}^2 + \Delta y_{n-1}^2 + \Delta z_{n-1}^2} \end{bmatrix} . \tag{5}$$

$$\begin{bmatrix} \Delta v_0 \\ \Delta v_1 \\ \vdots \\ \Delta v_{n-1} \end{bmatrix} = \begin{bmatrix} \dfrac{\Delta x_0 \Delta \dot{x}_0 + \Delta y_0 \Delta \dot{y}_0 + \Delta z_0 \Delta \dot{z}_0}{\Delta l_0} \\ \dfrac{\Delta x_1 \Delta \dot{x}_1 + \Delta y_1 \Delta \dot{y}_1 + \Delta z_1 \Delta \dot{z}_1}{\Delta l_1} \\ \vdots \\ \dfrac{\Delta x_{n-1} \Delta \dot{x}_{n-1} + \Delta y_{n-1} \Delta \dot{y}_{n-1} + \Delta z_{n-1} \Delta \dot{z}_{n-1}}{\Delta l_{n-1}} \end{bmatrix}. \tag{6}$$

Stiffness, damping, mass, and unloaded element length matrices are given as equations 7, 8, 9, and 10.

$$K = [k_0 \quad k_1 \quad \cdots \quad k_{n-1}]. \tag{7}$$

$$C = [c_0 \quad c_1 \quad \cdots \quad c_{n-1}]. \tag{8}$$

$$M = [m_0 \quad m_1 \quad \cdots \quad m_n]. \tag{9}$$

$$L = [l_0 \quad l_1 \quad \cdots \quad l_{n-1}]. \tag{10}$$

As shown in equation 11, the length of each tether element is equal to the total length divided by the number of tether beads, with the exception of the elements directly connected to the lead and follower projectiles which are given by equation 12.

$$l_i = \frac{l_t}{n-1}. \tag{11}$$

$$l_0 = \frac{l_0}{2}; \quad l_{n-1} = \frac{l_{n-1}}{2}. \tag{12}$$

With the previous definitions, the magnitudes of the tether forces are given in equations 13 and 14.

$$F_{T_i} = \begin{bmatrix} F_{T_0} & F_{T_1} & \cdots & F_{T_{n-1}} \end{bmatrix}. \tag{13}$$

$$F_{T_i} = \begin{Bmatrix} k_i(\Delta l_i - l_i) + c_i \Delta v_i, & \Delta l_i \geq l_i \\ 0, & \Delta l_i < l_i \end{Bmatrix}. \tag{14}$$

The elastic tether forces expressed in inertial coordinates are shown in equation 15.

$$\begin{Bmatrix} X_T \\ Y_T \\ Z_T \end{Bmatrix}_i = \frac{F_{T_i}}{\Delta l_i} \begin{Bmatrix} \Delta x_i \\ \Delta y_i \\ \Delta z_i \end{Bmatrix}. \tag{15}$$

The tether line forces exerted on adjacent masses are equal in magnitude and opposite in direction.

The follower projectile drag force is given in equation 16.

$$\begin{Bmatrix} X_D \\ Y_D \\ Z_D \end{Bmatrix}_n = -\frac{1}{2} \rho_n \sqrt{\dot{x}_n^2 + \dot{y}_n^2 + \dot{z}_n^2} A_n C_{D_n} \begin{Bmatrix} \dot{x} \\ \dot{y} \\ \dot{z} \end{Bmatrix}_n. \tag{16}$$

The projectile drag coefficients are Mach-number dependent and are computed by linear interpolation of tabulated data.

The aerodynamic force on the tether line includes skin friction drag along the tether line and flat plate drag perpendicular to the tether line [8]. To determine the tether drag, it is useful to define a unit vector, as shown in equation 17.

$$\begin{Bmatrix} r_x \\ r_y \\ r_z \end{Bmatrix}_i = \frac{1}{\Delta l_i} \begin{Bmatrix} \Delta x_i \\ \Delta y_i \\ \Delta z_i \end{Bmatrix}. \tag{17}$$

As shown in Figure 3, the tether line unit vectors are used to express the velocity of each bead into components along and normal to the adjacent drag elements. Note that the aerodynamic force acts on a bead even when the tether line is slack. The skin friction and flat plate drag for each element are given by equations 18 and 19.

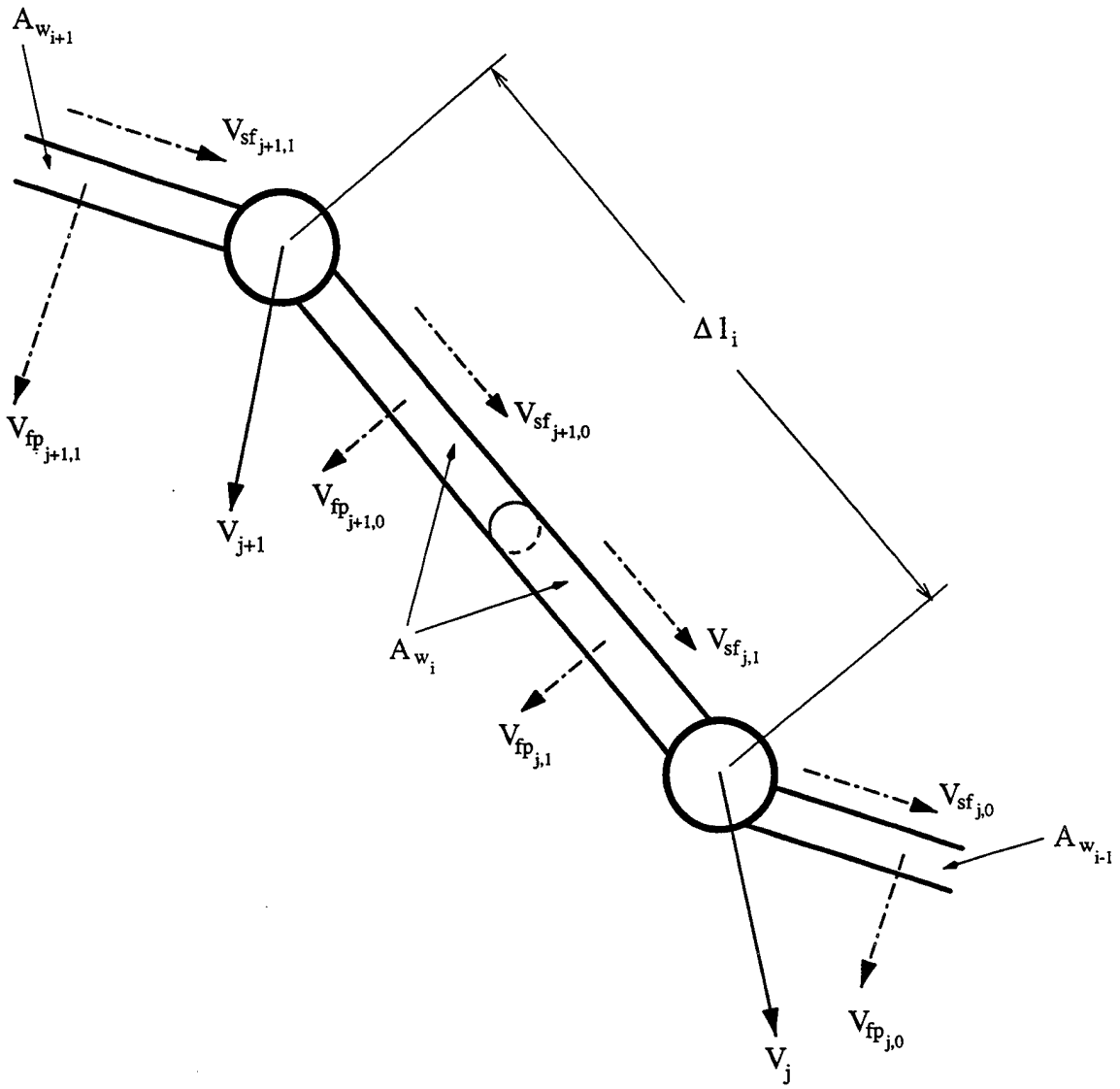

Figure 3. Aerodynamic Velocities Diagram.

$$D_{sf_{j,0}} = -\frac{1}{2}\rho_j \cdot A_{w_{i-1}} \cdot C_{sf} \cdot V_{sf_{j,0}} \cdot \left|V_{sf_{j,0}}\right|. \tag{18}$$

$$D_{fp_{j,0}} = -\frac{1}{2}\rho_j \cdot A_{w_{i-1}} \cdot C_{fp} \cdot \left(V_{fp_{j,0}}\right)^2. \tag{19}$$

The tether bead aerodynamic forces expressed in the inertial frame are shown in equation 20.

$$\begin{Bmatrix} X_D \\ Y_D \\ Z_D \end{Bmatrix}_j = D_{fp_{j,1}} \begin{Bmatrix} r_x \\ r_y \\ r_z \end{Bmatrix}_i + D_{fp_{j,0}} \begin{Bmatrix} r_x \\ r_y \\ r_z \end{Bmatrix}_{i-1} + \frac{D_{sf_{j,1}}}{V_{sf_{j,1}}} \begin{Bmatrix} V_{sf,x_{j,1}} \\ V_{sf,y_{j,1}} \\ V_{sf,z_{j,1}} \end{Bmatrix} + \frac{D_{sf_{j,0}}}{V_{sf_{j,0}}} \begin{Bmatrix} V_{sf,x_{j,0}} \\ V_{sf,y_{j,0}} \\ V_{sf,z_{j,0}} \end{Bmatrix}. \tag{20}$$

3. Tether Line Deployment Model

As the lead and follower projectiles separate, the tether line pays out. The two aspects to modeling this process are the pay out of the tether line from the lead projectile and the motion of released tether line. Two methods for modeling the released tether line motion were examined: the pop-out and all-out deployment methods.

The pop-out tether deployment model initially places all tether beads on the lead projectile. As the tether line is payed out, beads are released from the lead projectile into the atmosphere. A bead is not placed into the atmosphere until a sufficient length of line has been unreeled. Using the pop-out method, only a fraction of the tether beads are dynamically active in the atmosphere during deployment. When a bead is placed into the atmosphere, it is placed along the line from the release point to the last bead released, and initial conditions are established such that the elastic force across the line is unchanged. This tends to prevent a discontinuity in the line out rate due to bead release. However, because aerodynamic forces act on the bead immediately after it is released, a slight perturbation is generally observed when a bead is released. When a bead is released, the mass of the lead projectile is reduced by the released bead weight; the length

from the release point to the last tether bead released is reset along with the stiffness and damping coefficients of the exiting tether line.

The all-out tether deployment model places all beads into the atmosphere immediately after the projectiles are separated. The mass, stiffness, and damping characteristics of the tether line elements are continuously updated as the line is payed out. Initially, the mass of each bead is small and as line is released from the reel, the mass of each bead increases.

The tether reel is assumed to consist of a rotating reel acted on by the exiting bead elastic force. The elastic force between the lead object and the neighboring bead acts on the reel to pay out the tether line. The reel has a resistance force of 1 lb, which opposes the unreeling process. The equation governing the dynamics of the tether line unreeling process is shown in equations 21 and 22.

$$\ddot{s} = \frac{\left(F_{T_0} - F_r\right) r^2}{I_r}. \tag{21}$$

$$I_r = \frac{(m_r - ml \cdot s)^2}{2}. \tag{22}$$

When the full length of tether line has been reached, the acceleration and the velocity of the reel are set to zero.

4. Simulation Results

A key question for simulating the weapon system described is how many elements should be used to model the tether. As the number of degrees of freedom increases linearly with the number of beads, it is obviously desirable to use relatively few beads. To investigate this matter, the equations documented were simulated for varying tether discretizations. Typical values were selected for a 2,000-lb bomb lead projectile released from a fighter aircraft and a follower

projectile that is a sensor platform. Table 1 lists the nominal values used in the simulation. Figure 4 plots the maximum position error of the follower projectile as a function of the number of beads used to model the tether line. The reference trajectory used to compute the error at each time was the simulated trajectory using 200 beads. Because the lead projectile is much heavier than the follower projectile, its trajectory is modified much less than the follower projectile's

Table 1. Nominal Simulation Values

Projectile Follower Frontal Area	1.77 ft^2
Projectile Follower Weight	19.62 lb
Projectile Follower Initial Forward Velocity	500 ft/s
Projectile Follower Initial Vertical Velocity	0 ft/s
Projectile Follower Initial Side Velocity	0 ft/s
Projectile Lead Frontal Area	1.77 ft^2
Projectile Lead Weight	1,962 lb
Projectile Lead Initial Forward Velocity	500 ft/s
Projectile Lead Initial Vertical Velocity	0 ft/s
Projectile Lead Initial Side Velocity	0 ft/s
Coefficient of Drag Ratio (Follower/Lead)	2/1
Reel Radius	0.25 ft
Reel Weight	5 lb
Tether Length	1,000 ft
Tether Weight Per Unit Length	0.01 lb
Tether Diameter	0.0082 ft
Tether Stiffness	62,500 lb-ft/ft
Tether Damping Constant	0.30
Skin Friction Drag Coefficient	0.007
Flat Plate Drag Coefficient	1.100
Release Altitude	25,000 ft
Separation Time	0 s
Total Simulation Time	45 s

trajectory, with the addition of tether line coupling. For a low projectile mass ratio, follower projectile trajectory deviations represent the worst case. As shown in Figure 4, even for a small number of beads ($n \cong 10$), the maximum error in the follower trajectory is small. Using both tether deployment schemes, Figure 5 plots the maximum tether line force vs. the number of tether beads. For the configuration considered here, where the tether line is released from the

lead projectile, the maximum tether line load occurs shortly after the tether has fully deployed. This point is called the snatch load. Figure 5 shows a significant difference in the maximum tether line load between the all-out and pop-out methods. The all-out tether deployment scheme predicts significantly lower maximum loads than the pop-out method. The trend for the maximum acceleration of the follower is similar in nature to the maximum tether line load trend. In the pop-out method, beads are released into the atmosphere continuously during tether deployment. When a bead is released, aerodynamic forces immediately act on the bead and subsequently induce vibration throughout the tether line. This vibration wave along the tether line increases the maximum tether line load experienced during the event. Furthermore, Figure 5 shows that to predict the maximum line load, a large number of tether beads is required compared to predicting follower projectile position. Moreover, using a low number of tether beads to predict the maximum tether line force is nonconservative.

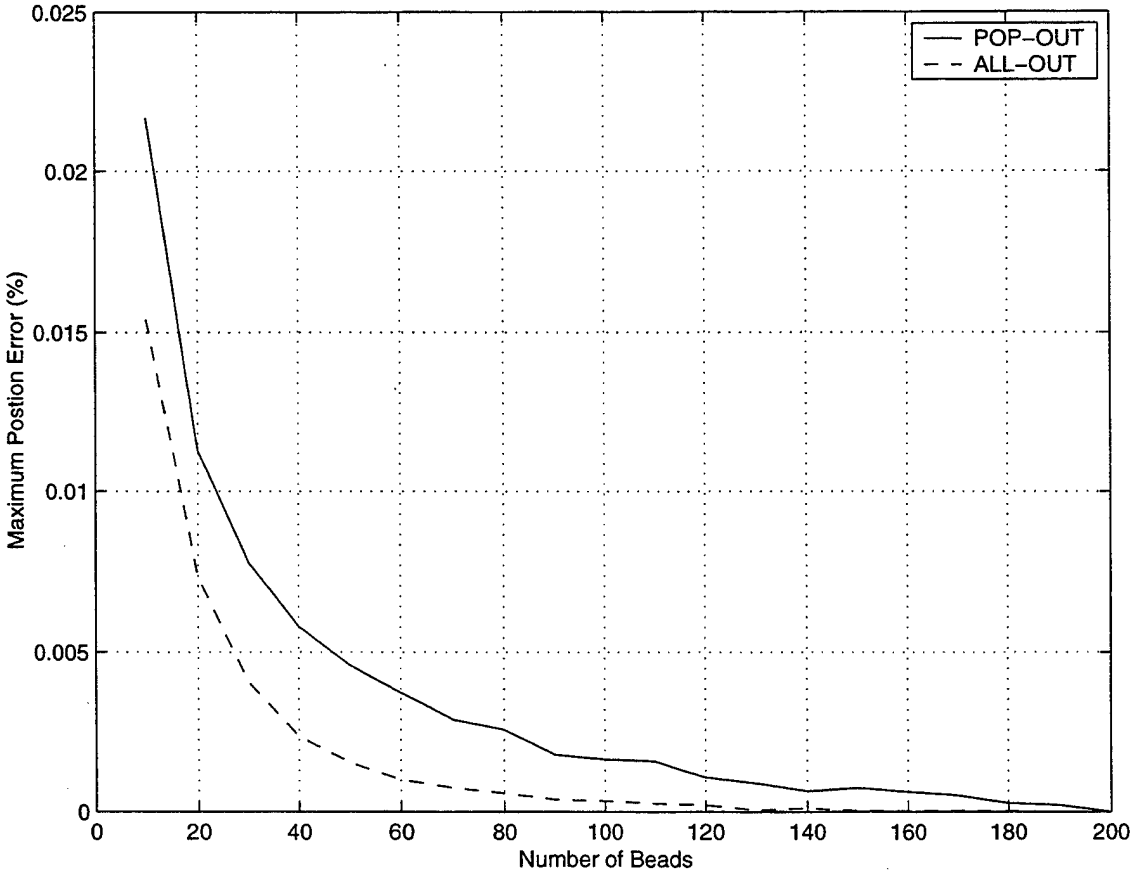

Figure 4. Maximum Position Error of Follower.

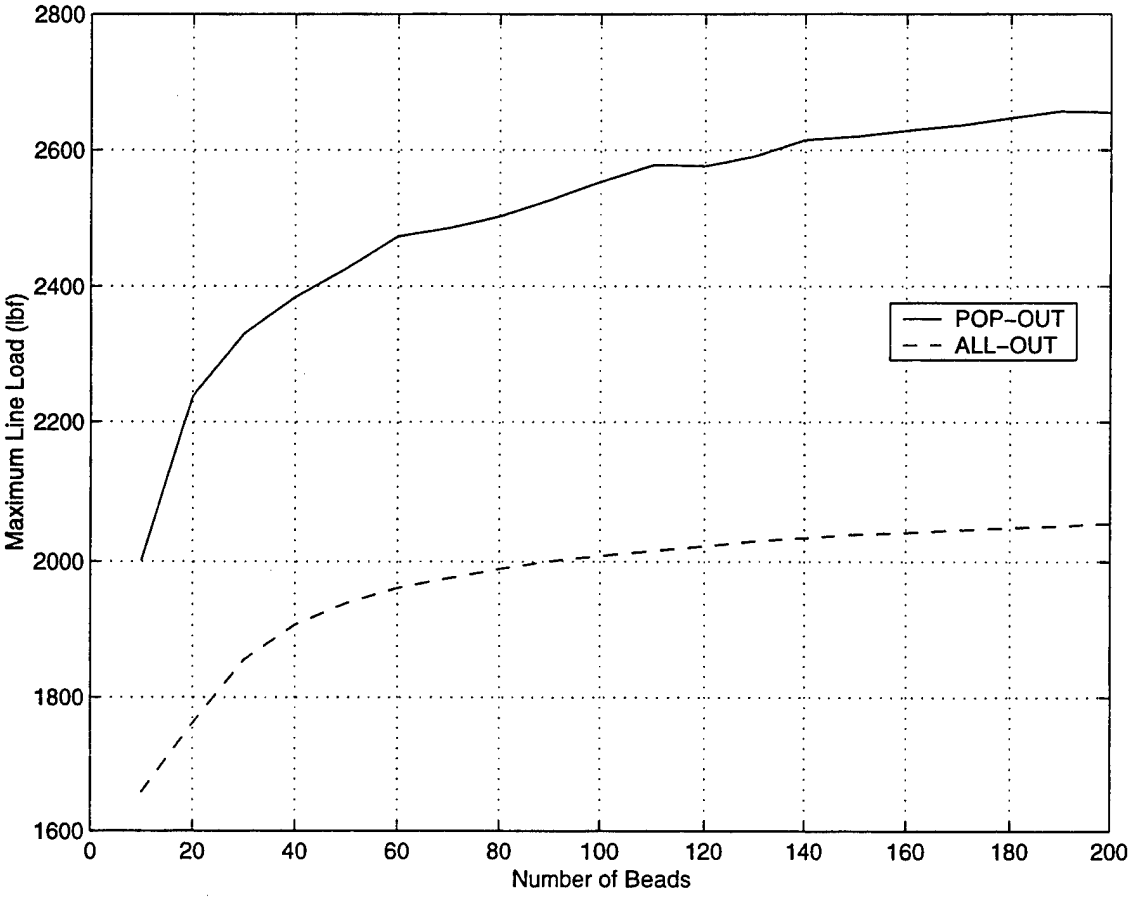

Figure 5. Maximum Line Load.

Because the all-out tether deployment method does not introduce spurious tether line vibration when releasing a bead, as the pop-out method does, modeling tether line deployment is seen as a superior technique. However, Figure 6 shows that the all-out tether deployment model incurs significantly higher computation time. Figure 6 plots the total number of time steps to perform a simulation vs. the number of tether beads. A fifth order Runge-Kutta adaptive time step numerical integration scheme was used to integrate the equations of motion. Figures 7 and 8 show the density of integration steps taken vs. time for the pop-out and all-out methods, respectively. In the all-out method, all beads are released into the atmosphere when the projectiles separate. Initially, only a small amount of line has been released from the reel, thus the bead mass is small and the equations of motion are relatively stiff. Typically, the numerical

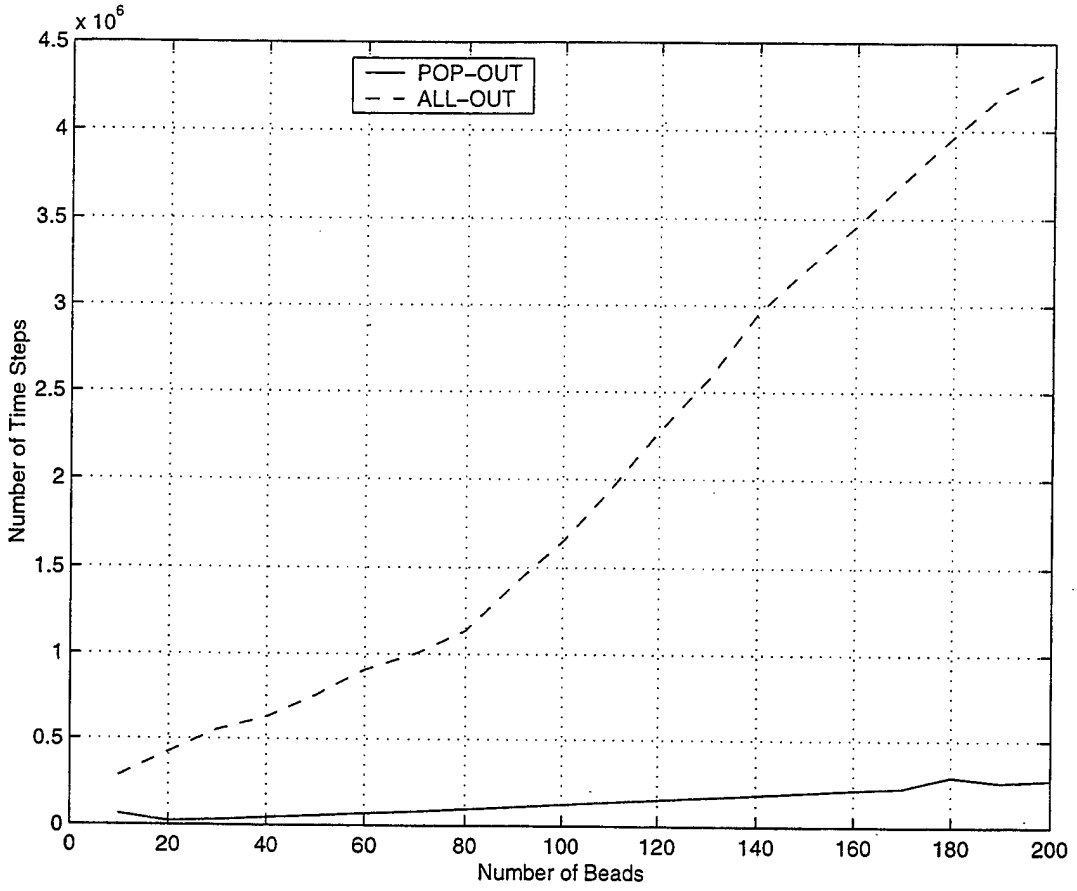

Figure 6. Total Number of Time Steps.

integrator significantly slows down immediately after the beads are released and also at the snatch load point. On the other hand, the pop-out method gradually releases beads as line is payed out. Hence, during deployment, the pop-out method integrates fewer equations of motion and has larger bead masses compared to the all-out method. The increase in steps near the end of the simulation is a result of the lead projectile hitting the ground.

5. Effect of Projectile Drag Coefficient Ratio for a Low Mass Ratio Configuration

The separation dynamics are driven in large part by the difference between the drag forces on the lead and follower projectiles. One of the primary questions designers are faced with is how to shape the follower projectile to unreel the tether line over a specified duration for time, while

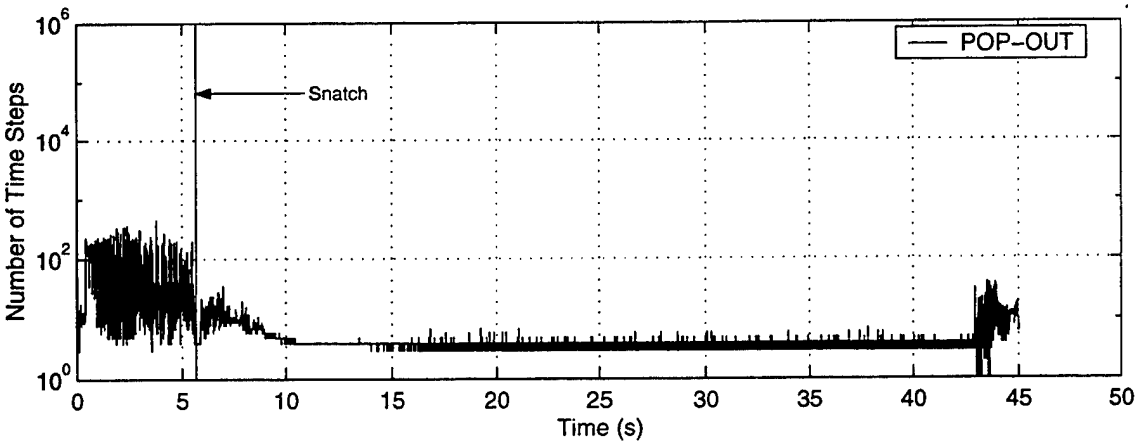

Figure 7. Number of Steps vs. Time for the Pop-Out Method.

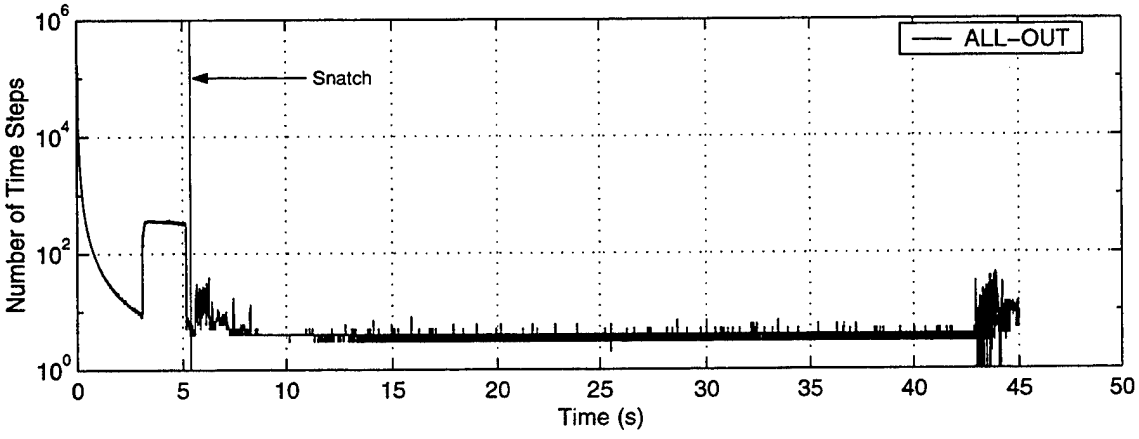

Figure 8. Number of Steps vs. Time for the All-Out Method.

at the same time limiting the tether line maximum loads and the follower projectile acceleration at the snatch point. This section shows the basic response for various projectile drag ratios when the follower projectile weight is 1% of the lead projectile. Figure 9 plots the range of the lead and follower projectiles for five different lead-to-follower drag coefficient ratios (1.25, 1.50, 1.75, 2.00, and 5.00). The shape of the drag coefficient curve vs. Mach number is identical for both projectiles. For a given drag coefficient ratio, the lead and follower trajectories overlay one another. As would be expected, a decrease in range is noticed when the follower projectile drag coefficient is increased. As shown in Figure 10, when the follower drag coefficient is increased, the tether line pays out more rapidly so that the tether line tension on the lead projectile is higher over a longer portion of the trajectory, which contributes to decreased range. For a drag coefficient ratio of 5.0, the decrease in range of 15% is substantial; however, the corresponding decrease in the tether deployment time is approximately 1 s.

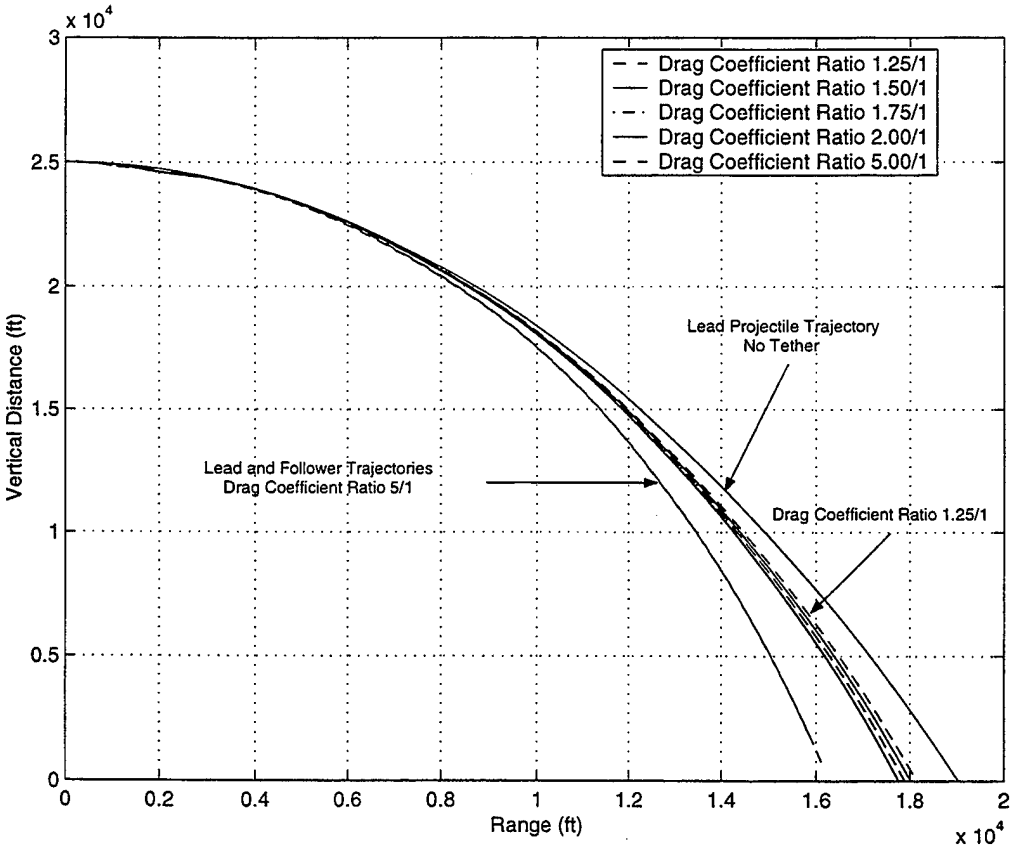

Figure 9. Range of Lead and Follower (Lead/Follower Mass Ratio 1%).

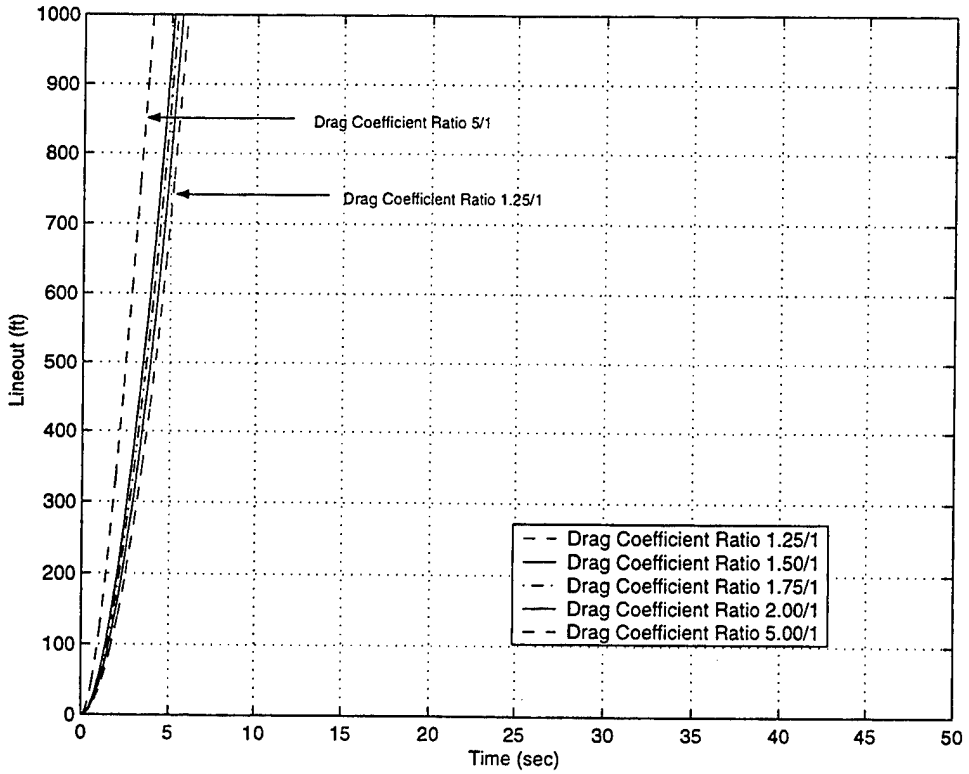

Figure 10. Lineout (Lead/Follower Mass Ratio 1%).

Figure 11 plots a sequence of frames that show the tether shape during a typical event for a low projectile mass ratio configuration. Notice that these results are for the pop-out method with a projectile drag coefficient ratio of 2.0. The lead projectile is on the right side and the follower projectile is on the left side of the tether line. The diamond on the tether line indicates where the maximum load in the tether line is located at that time instant. The line fully deploys in less than 5.67 s and hits the snatch load in frame 3. Notice the maximum line load is at the lead projectile. After the first snatch condition, the line goes slack and bunches (as shown in frames 4, 5, and 6).

The line encounters a second snatch condition at t = 7.83 s, as shown in frame 7. At the second snatch load condition, the maximum tether line load is at the follower projectile. As shown in frame 10, the projectile combination eventually settles into a steady-state drop by approximately t = 8.955 s. In frame 12, the lead projectile has already impacted the ground. The maximum tether line load moves back and forth along the tether line throughout the event. However, for this configuration the overall maximum line load occurs at the first snatch

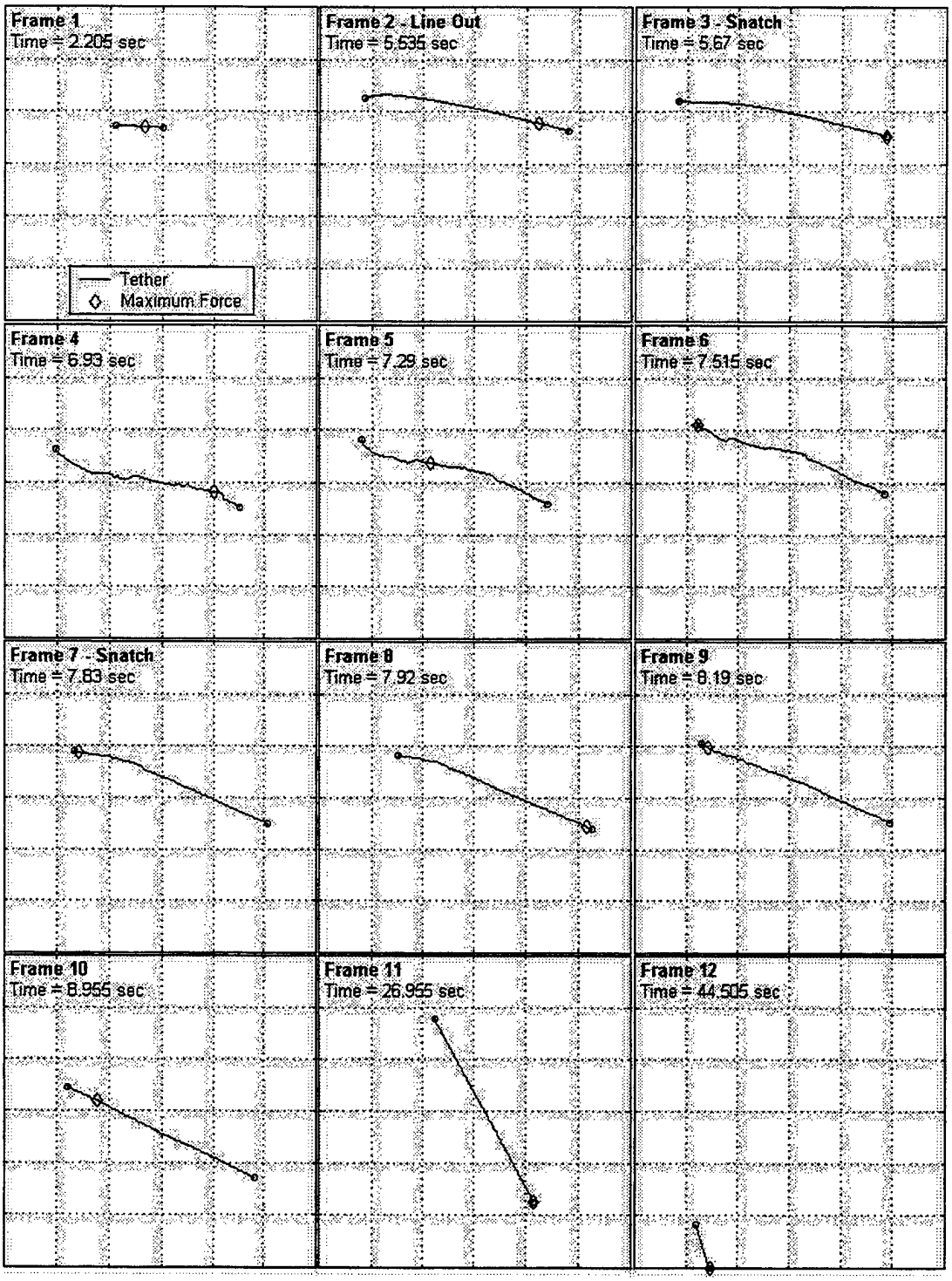

Figure 11. Pop-Out Method Tether Shape Sequence (Mass Ratio 1 %; Drag Ratio 2/1).

condition at the tether line and the lead projectile connection point. Figure 12 plots the magnitude of the inertial velocity of the lead projectile. For the configuration analyzed, the steady-state drop velocity is larger than the release velocity so the lead projectile increases its speed over the trajectory until it impacts the ground and its velocity goes to zero. As expected, when the follower projectile drag is increased, the lead projectile's speed is reduced and it takes longer to hit the ground. Figure 13 shows the speed of the follower projectile over the trajectory for different drag coefficient ratios. Notice that all traces show the same characteristics. Because the steady-state drop velocity of the follower projectile is lower than the aircraft release speed, the follower projectile initially slows down. The difference in speed between the lead and follower projectiles pays out the line.

When the tether line is fully deployed, the tether line grabs the follower and rapidly increases its speed. The follower then rebounds toward the lead projectile, so much that the tether line goes slack. With the line slack, the follower projectile again slows down to seek its steady-state drop velocity. This oscillation continues until a steady-state condition is arrived at where the lead and follower projectiles fall at the same speed. At the end of the trajectory, the lead projectile impacts the ground and shortly after the tether line goes slack; again, the follower projectile slows down and approaches its steady-state drop velocity. Figure 14 shows a bar graph of the maximum tether line tension for different drag coefficient ratios using both tether deployment methods. Notice that increasing the drag coefficient ratio increases the maximum tension. Thus, one must take care in selecting the drag coefficient ratio and avoid exceeding the ultimate line strength. Corresponding to Figure 14, Figure 15 shows the maximum acceleration of the follower projectile. The maximum acceleration also increases with an increased drag coefficient ratio.

6. Effect of Projectile Drag Coefficient Ratio for a High Mass Ratio Configuration

This section considers the system response for various projectile drag ratios when the weights of the follower and lead projectile are equal. The range of the lead and follower

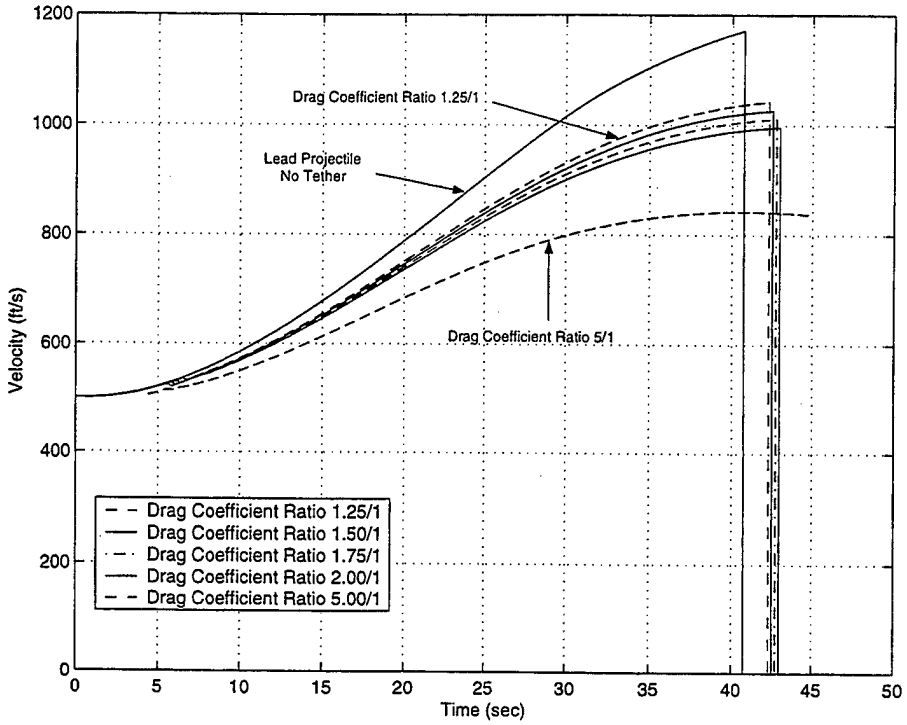

Figure 12. Speed of Lead Projectile (Lead/Follower Mass Ratio 1%).

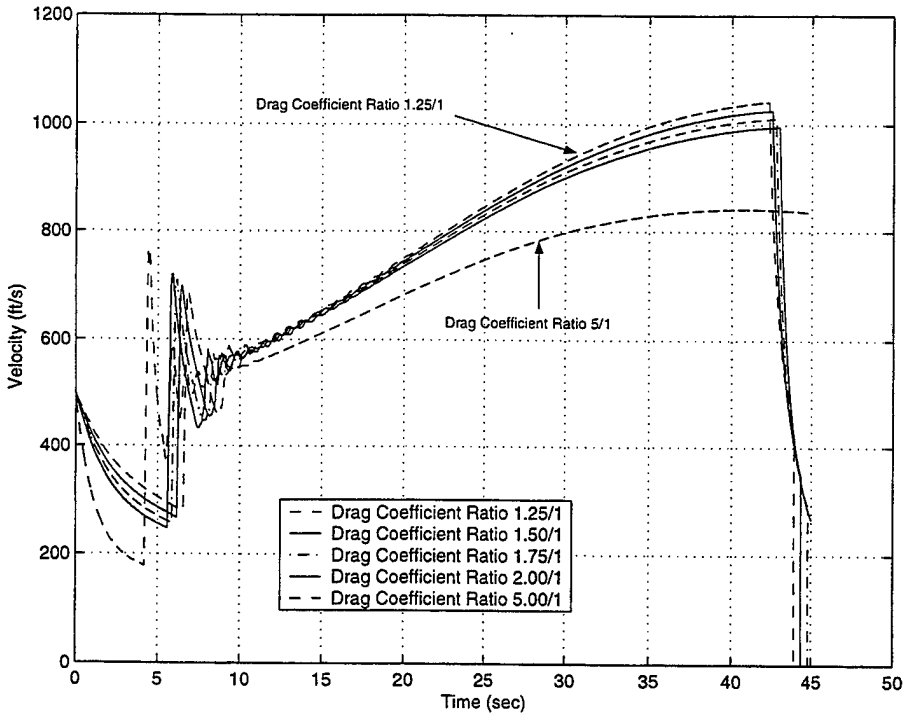

Figure 13. Speed of Follower Projecile (Lead/Follower Mass Ratio 1%).

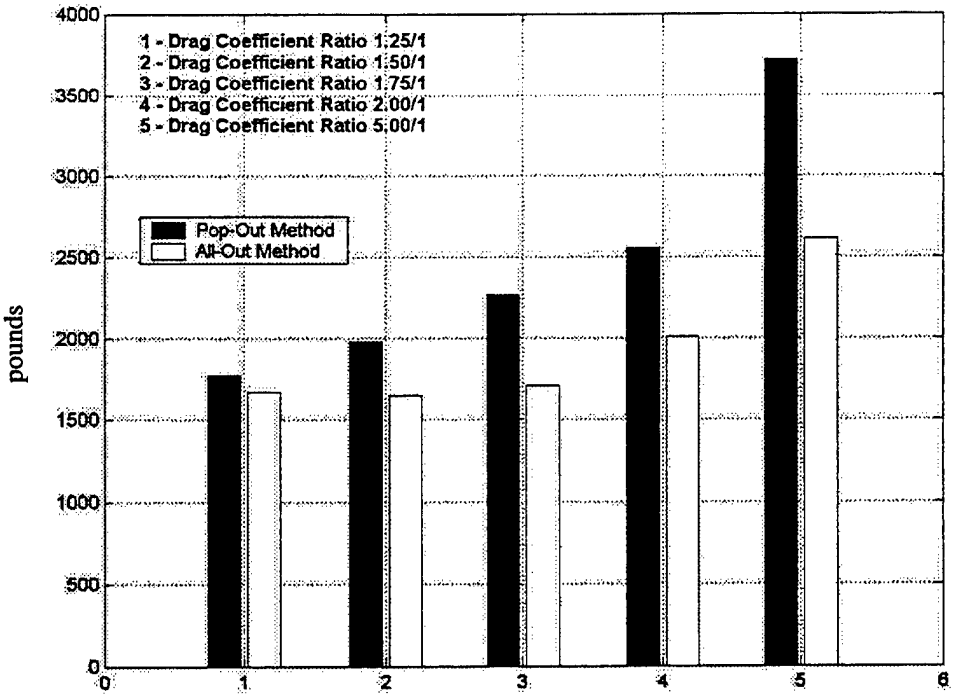

Figure 14. Maximum Line Load (Lead/Follower Mass Ratio 1%; 100 Beads).

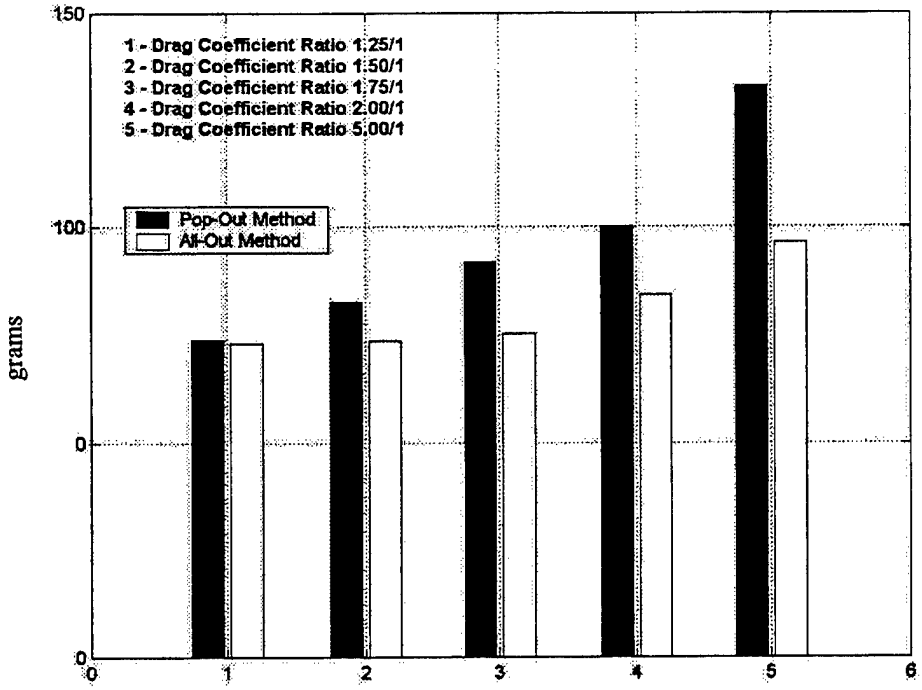

Figure 15. Maximum Acceleration of Follower (Lead/Follower Mass Ratio 1%; 100 Beads).

projectiles for the same five lead-to-follower drag coefficient ratios considered are plotted in Figure 16. For drag ratios of 1.75 and less, the tether line never becomes fully extended before the lead projectile contacts the ground and the lead and follower trajectories overlay one another. As with the 1% mass ratio study, a decrease in range is noticed when the follower projectile drag coefficient is increased. For drag coefficient ratios of 5.0 and 2.0, the lead and follower trajectories do not overlay one another because oscillations from snatch have not died out before the lead projectile comes in contact with the ground. As shown in Figure 17, when the follower drag coefficient is increased, the tether line pays out more rapidly. Except for the high drag coefficient ratios, this does not have the effect of reducing the range of the lead projectile as the 1% mass ratios did. Since the tether line for the low drag coefficient ratios never fully extends, the lead and follower projectiles approach their steady-state drop velocities with a slack tether line.

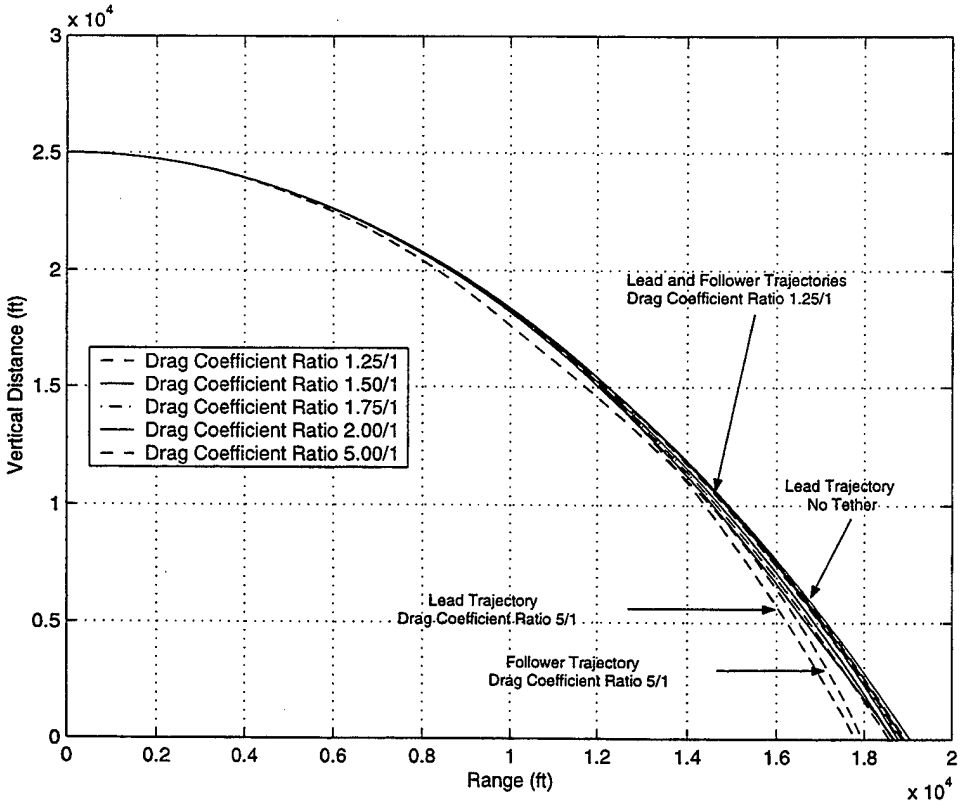

Figure 16. Range of Lead and Follower (Lead/Follower Mass Ratio 100%).

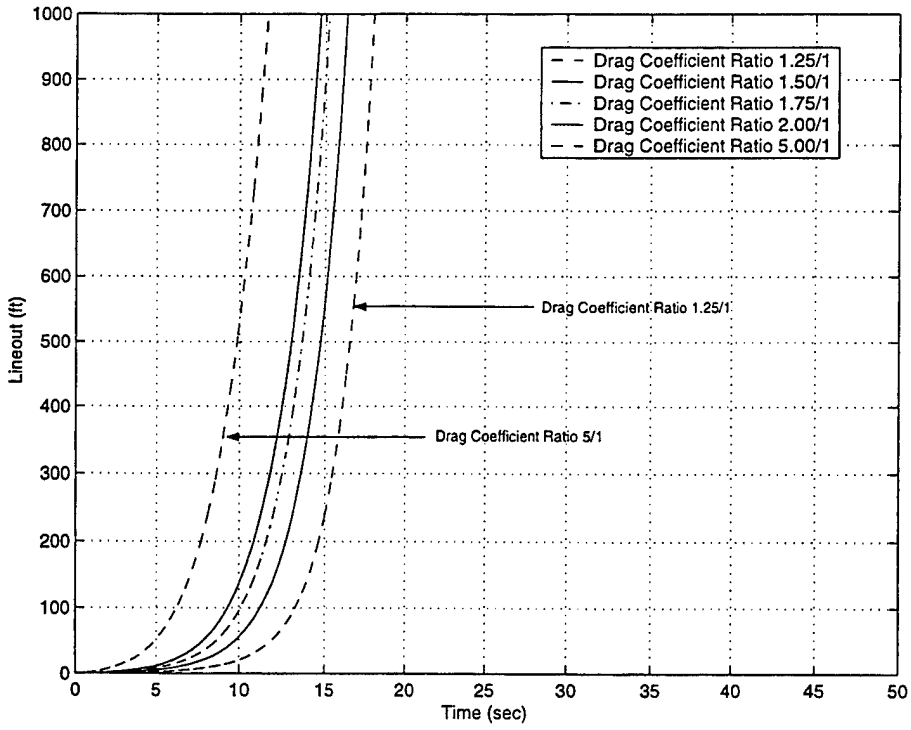

Figure 17. Lineout (Lead/Follower Mass Ratio 100%).

Figure 18 plots a sequence of frames that show the tether shape during a typical event for a high projectile mass ratio configuration. These results are for the pop-out method with a projectile drag coefficient ratio of 5.0. As before, the lead projectile is on the right side and the follower projectile is on the left side of the tether line. The diamond on the tether line indicates where the maximum load is on the tether line at that instant. In frame 1, the two projectiles begin to separate due to the drag on the follower projectile. As the tether is affected by aerodynamic drag, it begins to billow out in the shape shown in frame 2. Frames 3 and 4 show that the tether line is pulled out mainly due to the aerodynamic load on the exposed tether and not from the position difference of the follower and lead projectiles. It requires a relatively long time for the drag of the follower to overcome its momentum; consequently, snatch does not occur until approximately 23.94 s in frame 5. As with the 1% mass ratio case, the maximum line load occurs between the connection point of the lead projectile and the first bead. After snatch, the tether line reacts differently than the 1% mass ratio configuration. Instead of the tether bunching, a whipping action is imparted to the tether and the follower increases in velocity

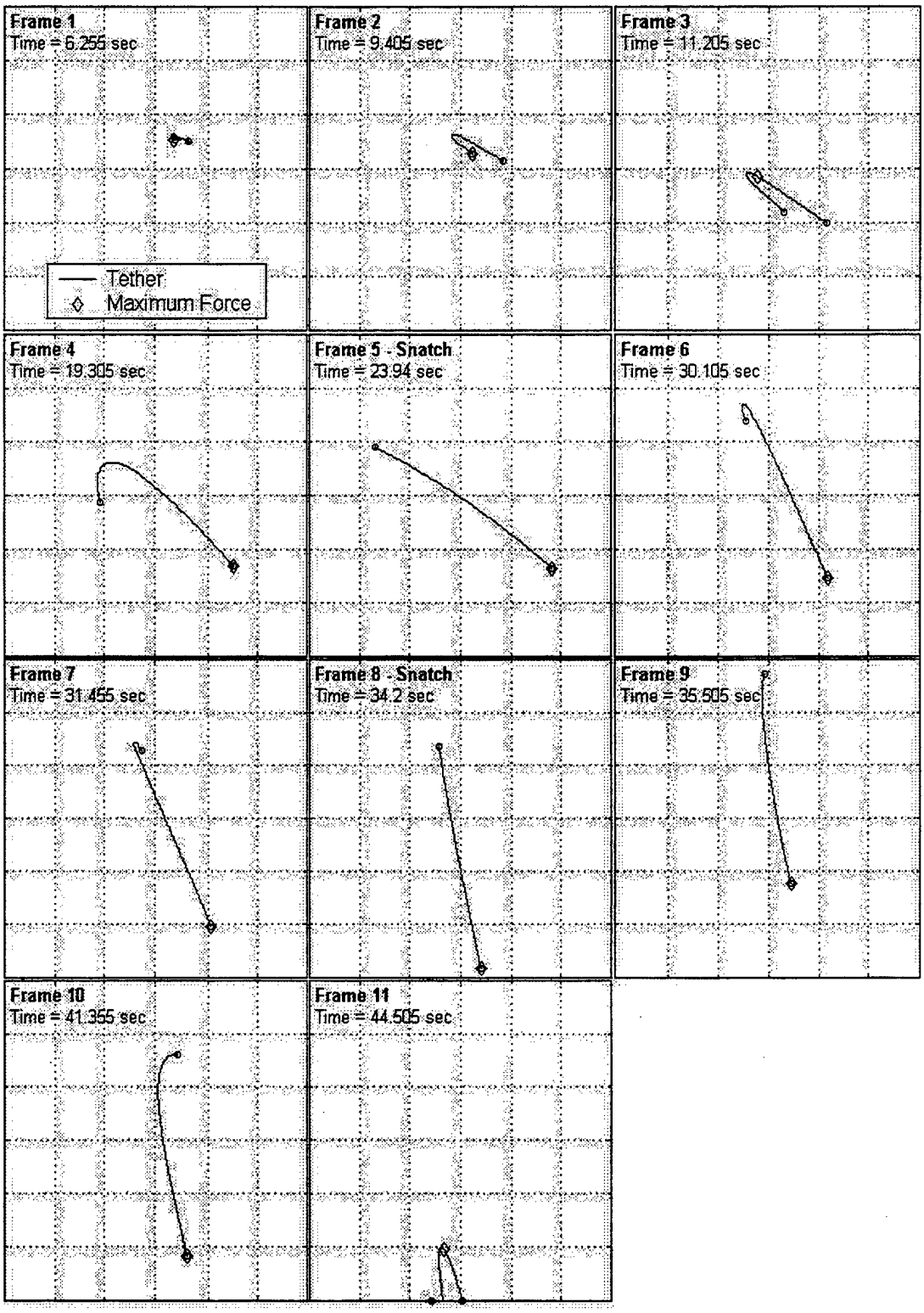

Figure 18. Pop-Out Method Tether Shape Sequence (Mass Ratio 100%; Drag Ratio 2/1).

as it swings downward and then again upward through the line (as shown in frames 6 and 7). This action creates the potential for the entanglement of the tether line. As shown in frame 8, snatch occurs again at approximately 34.2 s and the maximum line load is again at the connection point. This is the point in time at which the overall maximum line load occurs, and not at the initial snatch point. Frame 9 shows that the snatch load causes the follower to fly forward in an upward swing. As the projectiles approach the ground in frame 10, the follower is significantly ahead of an extended trailing position that is achieved for the 1% mass ratio configuration. Frame 11 shows that the follower projectile lands past the lead when the two projectiles come in contact with the ground. Figure 19 plots the magnitude of the inertial velocity of the lead projectile. Unlike the low projectile mass ratio case, the lead projectile's speed is greatly affected by the snatch load for the drag coefficient ratio of 5.0. The other traces do not exhibit this characteristic because snatch does not occur, or occurs just prior to the lead projectile hitting the ground. Figure 20 demonstrates the increases in the speed of the follower due to the whipping actions presented in Figure 18 for the drag coefficient ratio of 5.0. The lead and follower projectiles never enter into a steady-state condition, as in the 1% mass ratio case.

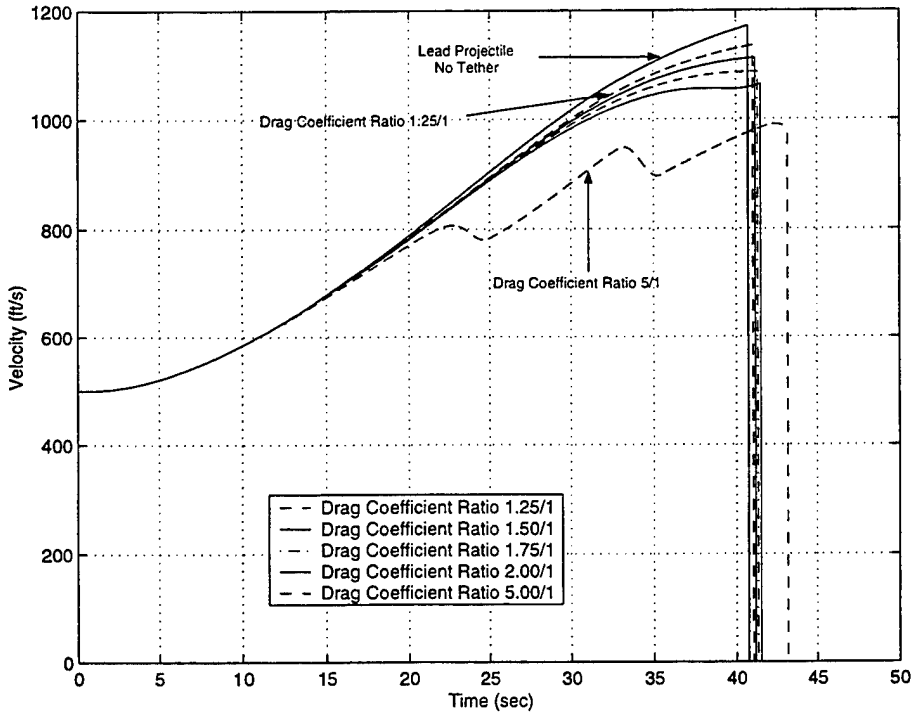

Figure 19. Speed of Lead Projectile (Pop-Out Method - Lead/Follower Mass Ratio 100%).

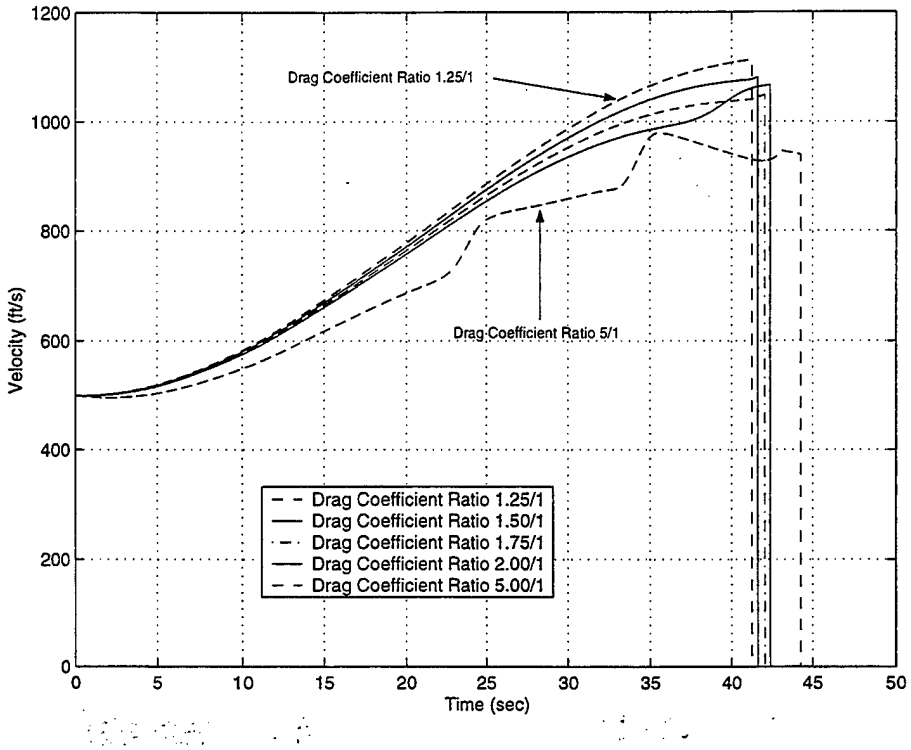

Figure 20. Speed of Follower Projectile (Pop-Out Method - Lead/Follower Mass Ratio 100%).

7. Effect of Tether Stiffness for a Low Mass Ratio Configuration

This section shows the basic response for various tether stiffness values when the follower projectile weight is 1% of the lead projectile. Figure 21 plots the range of the lead and follower projectiles for 5 different stiffness values (10,000 lb-ft/ft, 25,000 lb-ft/ft, 50,000 lb-ft/ft, 62,500 lb-ft/ft, and 75,000 lb-ft/ft). As shown in Figure 21, all the trajectories coincide, indicating that the tether stiffness has no noticeable effect on the range of the lead and follower projectiles. Figure 22 shows that the same is true for the lineout rate. Figure 23 shows the speed of the lead projectile for various tether stiffness values. Except for a slight decrease at the point of snatch, the tether stiffness has no effect on the lead projectile's speed either. The speed of the follower projectile is plotted in Figure 24. A decrease in tether stiffness allows the oscillations caused by snatch to persist for a slightly longer period of time. However, even for a stiffness value of 10,000 lb-ft/ft, the oscillations die out and a steady-state condition is achieved at approximately

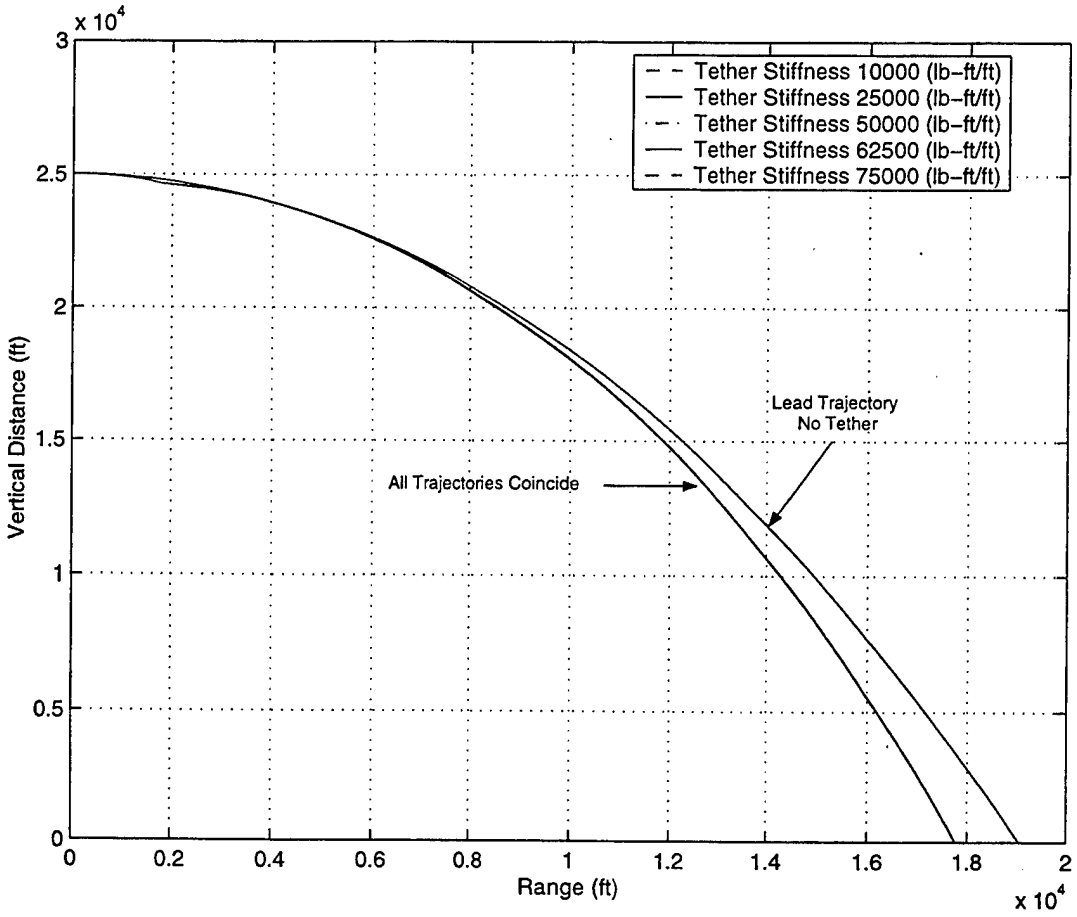

Figure 21. Range of Lead and Follower (Lead/Follower Mass Ratio 1%).

18 s into the flight. Figure 25 shows a bar graph of the maximum tether line tension for different tether stiffness values using both deployment methods. Notice that increasing the tether stiffness increases the maximum tension. A corresponding graph is shown in Figure 26 for the maximum acceleration of the follower projectile. These two graphs demonstrate that in order to decrease both maximum line loads and the g forces on the follower projectile, tether stiffness should be minimized.

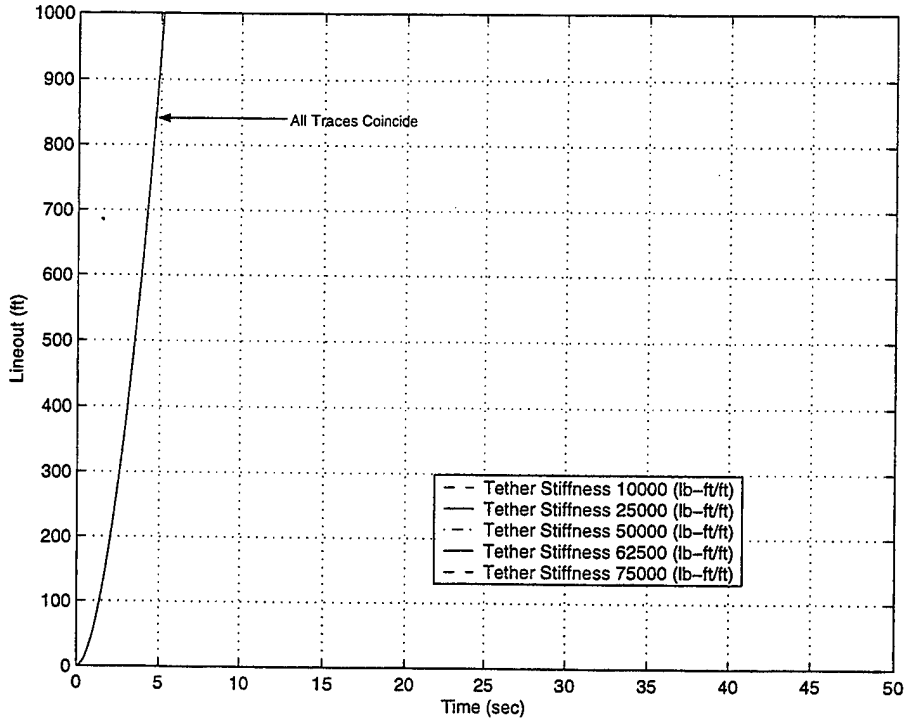

Figure 22. Lineout (Lead/Follower Mass Ratio 1%).

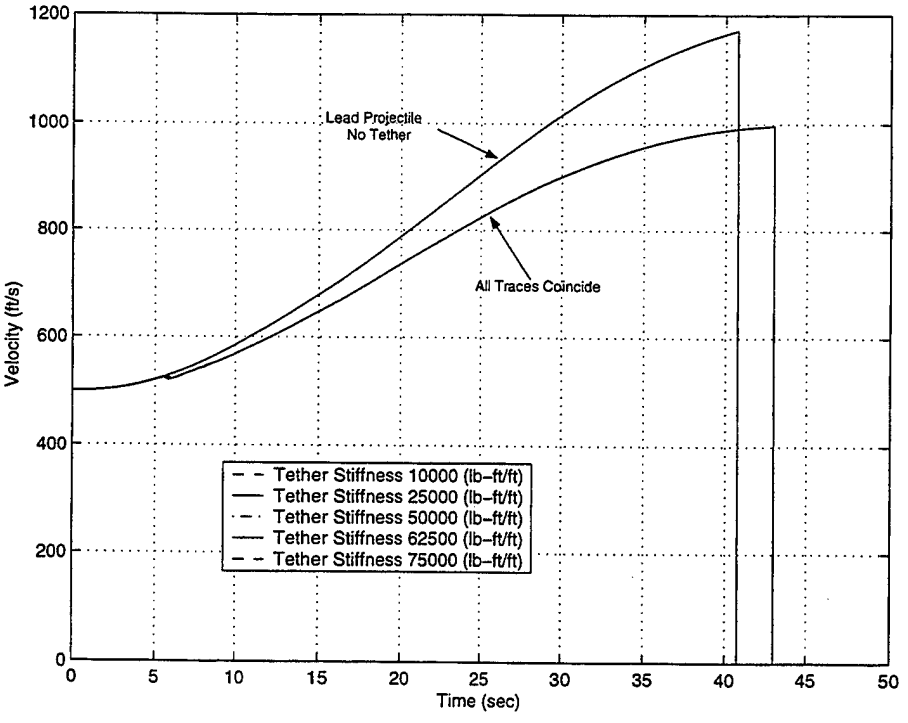

Figure 23. Speed of Lead Projectile (Lead/Follower Mass Ratio 1%).

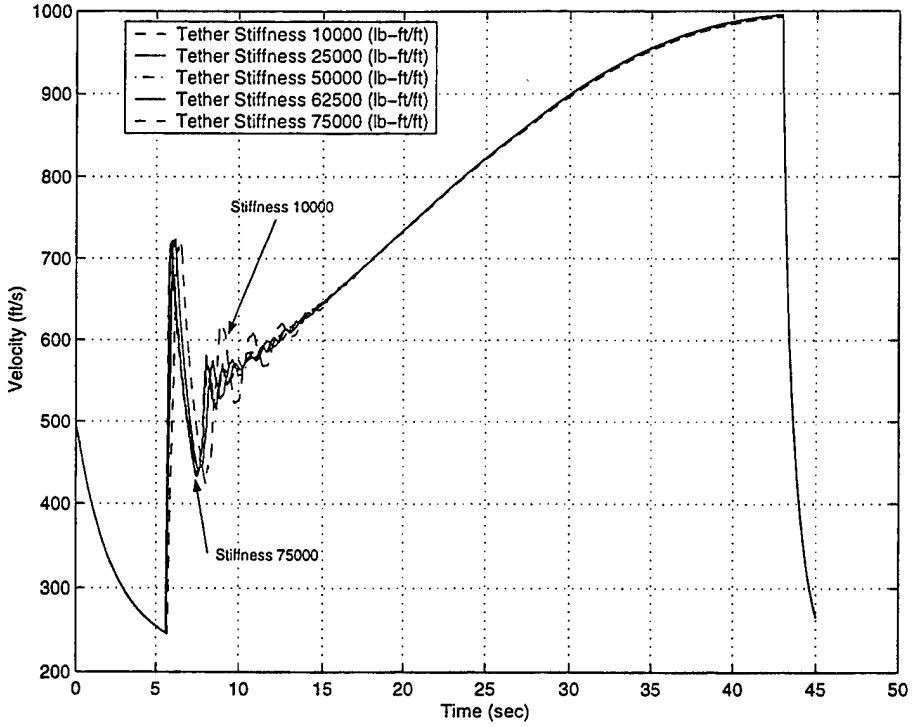

Figure 24. Speed of Follower Projectile (Lead/Follower Mass Ratio 1%).

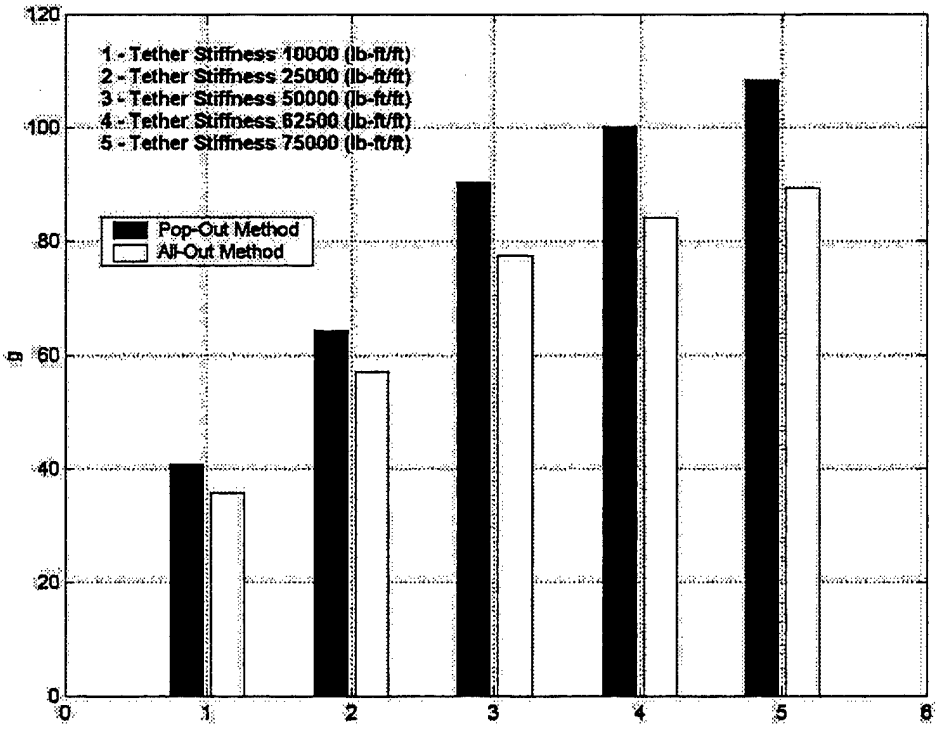

Figure 25. Maximum Line Load (Lead/Follower Mass Ratio 1%; 100 Beads).

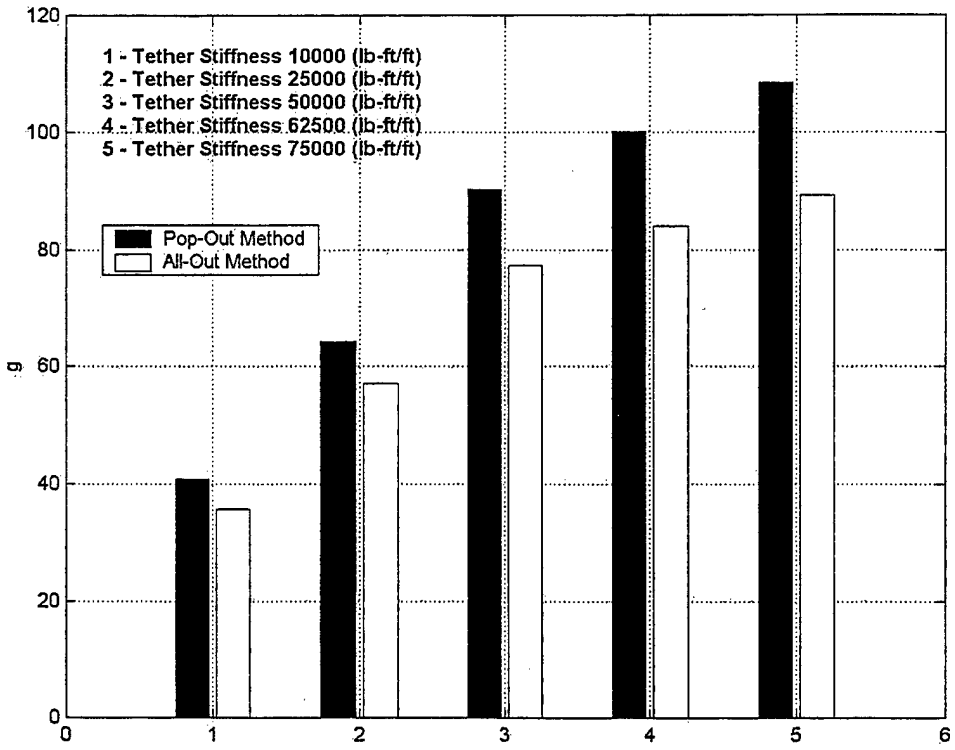

Figure 26. Maximum Acceleration of Follower (Lead/Follower Mass Ratio 1%; 100 Beads).

8. Conclusions

A dynamic model was developed in order to study the dynamics of two projectiles that are connected by a tether line. Two methods of modeling tether line deployment were studied. The pop-out method, which gradually releases beads into the atmosphere, is numerically more efficient but has the disadvantage of introducing tether vibration when beads are released. The all-out method requires significant computation time since when all beads are initially released, the bead masses are very small and the equations of motion are relatively stiff. This problem can be avoided by initially deploying enough line so that the equations can be efficiently integrated. While the position trajectories converge for less than 10 tether bead elements, the convergence for maximum tether line force requires more than 100 elements. If this munition system is being simulated solely to obtain trajectory information, then a model that utilizes a low number of beads (< 10) is sufficient. On the other hand, if the simulation tool is going to be used for

trajectory calculations and internal loads estimation, then a much higher order system must be used (> 100).

Simulation results for the different follower-to-lead projectile weight ratio shows that different mechanisms unreel the tether line depending on the follower projectile weight. For a low follower-to-lead projectile mass ratio, the tether line is unreeled by the difference in position between the projectiles. For a high mass ratio, the tether line aerodynamic force unreels the tether line. Hence, the tether line unreels itself.

Although the tether line stiffness has very little affect on the position dynamics, it does strongly influence dynamic loading. From a design standpoint, a low stiffness, high ultimate strength tether material is most desirable. Proper tether material selection must consider both ultimate line strength and tether stiffness because they affect loads. For a low-mass ratio configuration, an increase in the follower-to-lead projectile drag coefficient ratio has the expected effect of decreasing tether line deployment time and increasing tether line loads and follower projectile maximum acceleration.

9. References

1. Tye, G., and R. Han. "Attitude Dynamics Investigation of the OEDIPUS - A Tethered Rocket Payload." *Journal of Spacecraft and Rockets*, vol. 32, no. 1, 1995.

2. Puig-Suari, J., J. Longuski, and S. Tragesser. "Aerocapture With a Flexible Tether." *Journal of Guidance, Control, and Dynamics*, vol. 18, no. 6, 1995.

3. No, T. S., and J. E. Cochran. "Dynamics and Control of a Tethered Flight Vehicle." *Journal of Guidance, Control, and Dynamics*, vol. 18, no. 1, 1995.

4. Clifton, J. M., L. V. Schmidt, and T. D. Stuart. "Dynamic Modeling of a Trailing Wire Towed by an Orbiting Aircraft." *Journal of Guidance, Control, and Dynamics*, vol. 18, no. 4, 1995.

5. Doyle, G. R., Jr. "Mathematical Model for the Ascent and Descent of a High-Altitude Tethered Balloon." *J. Aircraft*, vol. 6, no. 5, pp. 457–462, September–October 1969.

6. Matthews, W. "Camera May Relay Instant Images of Bomb Damage." *Airforce Times*, vol. 30, August 1997.

7. Von Mises, R. *Theory of Flight.* New York: Dover Publications Inc., 1959.

8. Djerassi, S. Personal communication, 1997.

INTENTIONALLY LEFT BLANK.

List of Symbols

x_j, y_j, z_j	Position vector components of the *jth* bead in the inertial reference frame.
X_A, Y_A, Z_A	Drag force in the inertial reference frame for fully deployed model.
X_{T_i}, Y_{T_i}, Z_{T_i}	Elastic line force of the *ith* element in the inertial reference frame.
W_j	Weight of the *jth* bead.
ρ_n	Air density at the altitude of the follower object.
A_n	Projected area of the follower object.
A_{w_i}	Wetted area of the *ith* element.
A_{c_i}	Cross-sectional area of the *ith* element.
$V_{sf_{j,1}}$	Velocity of the *jth* bead normal to *ith* tether element.
$V_{sf_{j,0}}$	Velocity of the *jth* bead normal to *ith*-1 tether element.
$V_{fp_{j,1}}$	Velocity of the *jth* bead parallel to *ith* tether element.
$V_{fp_{j,0}}$	Velocity of the *jth* bead parallel to *ith*-1 tether element.
$D_{sf_{j,1}}$	Skin friction drag force applied to the *jth* bead due to the *ith* tether element.
$D_{sf_{j,0}}$	Skin friction drag force applied to the *jth* bead due to the *ith*-1 tether element.
$D_{fp_{j,1}}$	Flat plate drag force applied to the *jth* bead due to the *ith* tether element.
$D_{fp_{j,0}}$	Flat plate drag force applied to the *jth* bead due to the *ith*-1 tether element.
Cd_n	Coefficient of drag for the follower object.
C_{sf}	Coefficient of the skin friction drag.
C_{fp}	Coefficient of the flat plate drag.
r_i	Unit vector of the *ith* element.
Δx_j, Δy_j, Δz_j	Position difference between each node for the *jth* element in the inertial reference frame.
$\Delta \dot{x}_j$, $\Delta \dot{y}_j$, $\Delta \dot{z}_j$	Velocity difference between each node for the *jth* element in the inertial reference frame.
Δl_i	Distance between each node for the *ith* element.
Δv_i	Magnitude of the velocity difference between each node for the *ith* element.
k_i	Stiffness coefficient for the *ith* element.
c_i	Damping coefficient for the *ith* element.
m_j	Mass of the *jth* bead.
m_r	Mass of the reel.
ml	Tether line mass per unit length.

l_b	Length of tether assigned to each mass.
l_i	Unstretched length of the *ith* element.
F_{T_j}	Magnitude of the elastic line force for the *jth* element.
s	Total length of tether line out.
$\ddot{s}$	Acceleration of the exiting tether line.
F_r	Resistance force of the reel.
I_r	Mass moment of inertia for the reel.
r	Radius of the reel.
n	Number of the follower object.
i	Bead index.
j	Line element index.

NO. OF COPIES	ORGANIZATION
2	DEFENSE TECHNICAL INFORMATION CENTER DTIC DDA 8725 JOHN J KINGMAN RD STE 0944 FT BELVOIR VA 22060-6218
1	HQDA DAMO FDT 400 ARMY PENTAGON WASHINGTON DC 20310-0460
1	OSD OUSD(A&T)/ODDDR&E(R) R J TREW THE PENTAGON WASHINGTON DC 20301-7100
1	DPTY CG FOR RDA US ARMY MATERIEL CMD AMCRDA 5001 EISENHOWER AVE ALEXANDRIA VA 22333-0001
1	INST FOR ADVNCD TCHNLGY THE UNIV OF TEXAS AT AUSTIN PO BOX 202797 AUSTIN TX 78720-2797
1	DARPA B KASPAR 3701 N FAIRFAX DR ARLINGTON VA 22203-1714
1	NAVAL SURFACE WARFARE CTR CODE B07 J PENNELLA 17320 DAHLGREN RD BLDG 1470 RM 1101 DAHLGREN VA 22448-5100
1	US MILITARY ACADEMY MATH SCI CTR OF EXCELLENCE DEPT OF MATHEMATICAL SCI MADN MATH THAYER HALL WEST POINT NY 10996-1786

NO. OF COPIES	ORGANIZATION
1	DIRECTOR US ARMY RESEARCH LAB AMSRL D D R SMITH 2800 POWDER MILL RD ADELPHI MD 20783-1197
1	DIRECTOR US ARMY RESEARCH LAB AMSRL DD 2800 POWDER MILL RD ADELPHI MD 20783-1197
1	DIRECTOR US ARMY RESEARCH LAB AMSRL CS AS (RECORDS MGMT) 2800 POWDER MILL RD ADELPHI MD 20783-1145
3	DIRECTOR US ARMY RESEARCH LAB AMSRL CI LL 2800 POWDER MILL RD ADELPHI MD 20783-1145
	ABERDEEN PROVING GROUND
4	DIR USARL AMSRL CI LP (BLDG 305)

NO. OF COPIES	ORGANIZATION
3	AIR FORCE RSRCH LAB MUNITIONS DIR AFRL/MNAV G ABATE 101 W EGLIN BLVD STE 219 EGLIN AFB FL 32542
3	ALLEN PETERSON 159 S HIGHLAND DR KENNEWICK WA 99337
1	CDR WL/MNMF D MABRY 101 W EGLIN BLVD STE 219 EGLIN AFB FL 32542-6810
20	OREGON STATE UNIVERSITY DEPT OF MECHL ENGRG M COSTELLO CORVALLIS OR 97331
4	CDR US ARMY ARDEC AMSTA AR CCH J DELORENZO S MUSALI R SAYER P DONADIO PICATINNY ARESENAL NJ 07806-5000
7	CDR US ARMY TANK MAIN ARMAMENT SYSTEM AMCPM TMA D GUZIEWICZ R DARCEY C KIMKER R JOINSON E KOPOAC T LOUZIERIO C LEVECHIA PICATINNY ARESENAL NJ 07806-5000
1	CDR USA YUMA PROV GRND STEYT MTW YUMA AZ 85365-9103

NO. OF COPIES	ORGANIZATION
10	CDR US ARMY TACOM AMCPEO HFM AMCPEO HFM F AMCPEO HFM C AMCPM ABMS AMCPM BLOCKIII AMSTA CF AMSTA Z AMSTA ZD AMCPM ABMS S W DR PATTISON A HAVERILLA WARREN MI 48397-5000
1	DIR BENET LABORATORIES SMCWV QAR T MCCLOSKEY WATERVLIET NY 12189-5000
1	CDR USAOTEA CSTE CCA DR RUSSELL ALEXANDRIA VA 22302-1458
2	DIR US ARMY ARMOR CTR & SCHL ATSB WP ORSA A POMEY ATSB CDC FT KNOX KY 40121
1	CDR US ARMY AMCCOM AMSMC ASR A MR CRAWFORD ROCK ISLAND IL 61299-6000
2	PROGRAM MANAGER GROUND WEAPONS MCRDAC LTC VARELA CBGT QUANTICO VA 22134-5000

NO. OF COPIES	ORGANIZATION
4	COMMANDER US ARMY TRADOC ATCD T ATCD TT ATTE ZC ATTG Y FT MONROE VA 23651-5000
1	NAWC F PICKETT CODE C2774 CLPL BLDG 1031 CHINA LAKE CA 93555
1	NAVAL ORDNANCE STATION ADVNCD SYS TCHNLGY BRNCH D HOLMES CODE 2011 LOUISVILLE KY 40214-5001
1	NAVAL SURFACE WARFARE CTR F G MOORE DAHLGREN DIVISION CODE G04 DAHLGREN VA 22448-5000
1	US MILITARY ACADEMY MATH SCI CTR OF EXCELLENCE DEPT OF MATHEMATICAL SCI MDN A MAJ DON ENGEN THAYER HALL WEST POINT NY 10996-1786
3	DIR SNL A HODAPP W OBERKAMPF F BLOTTNER DIVISION 1631 ALBUQUERQUE NM 87185
3	ALLIANT TECH SYSTEMS C CANDLAND R BURETTA R BECKER 7225 NORTHLAND DR BROOKLYN PARK MN 55428

NO. OF COPIES	ORGANIZATION
3	DIR USARL AMSRL SE RM H WALLACE AMSRL SS SM J EIKE A LADAS 2800 POWDER MILL RD ADELPHI MD 20783-1145
1	OFC OF ASST SECY OF ARMY FOR R&D SARD TR W MORRISON 2115 JEFFERSON DAVIS HWY ARLINGTON VA 22202-3911
2	CDR USARDEC AMSTA FSP A S DEFEO R SICIGNANO PICATINNY ARESENAL NJ 07806-5000
2	CDR USARDEC AMSTA AR CCH A M PALATHINGAL R CARR PICATINNY ARESENAL NJ 07806-5000
5	TACOM ARDEC AMSTA AR FSA K CHIEFA AMSTA AR FS A WARNASCH AMSTA AR FSF W RYBA AMSTA AR FSP S PEARCY J HEDDERICH PICATINNY ARESENAL NJ 07806-5000

NO. OF COPIES	ORGANIZATION
5	CDR US ARMY MICOM AMSMI RD P JACOBS P RUFFIN AMSMI RD MG GA C LEWIS AMSMI RD MG NC C ROBERTS AMSMI RD ST GD D DAVIS RSA AL 35898-5247
3	CDR US ARMY AVN TRP CMD DIRECTORATE FOR ENGINEERING AMSATR ESW M MAMOUD M JOHNSON J OBERMARK RSA AL 35898-5247
1	DIR US ARMY RTTC STERT TE F TD R EPPS BLDG 7855 RSA AL 35898-8052
2	STRICOM AMFTI EL D SCHNEIDER R COLANGELO 12350 RESEARCH PKWY ORLANDO FL 32826-3276
1	CDR OFFICE OF NAVAL RES CODE 333 J GOLDWASSER 800 N QUINCY ST RM 507 ARLINGTON VA 22217-5660
1	CDR US ARMY RES OFFICE AMXRO RT IP TECH LIB PO BOX 12211 RESEARCH TRIANGLE PARK NJ 27709-2211

NO. OF COPIES	ORGANIZATION
4	CDR US ARMY AVN TRP CMD AVIATION APPLIED TECH DIR AMSATR TI R BARLOW E BERCHER T CONDON B TENNEY FT EUSTIS VA 23604-5577
3	CDR NAWC WEAPONS DIV CODE 543400D S MEYERS CODE C2744 T MUNSINGER CODE C3904 D SCOFIELD CHINA LAKE CA 93555-6100
1	CDR NSWC CRANE DIVISION CODE 4024 J SKOMP 300 HIGHWAY 361 CRANE IN 47522-5000
1	CDR NSWC DAHLGREN DIV CODE 40D J BLANKENSHIP 6703 WEST HWY 98 PANAMA CITY FL 32407-7001
1	CDR NSWC J FRAYSEE D HAGEN 17320 DAHLGREN RD DAHLGREN VA 22448-5000

NO. OF COPIES	ORGANIZATION
5	CDR NSWC INDIAN HEAD DIV CODE 40D D GARVICK CODE 4110C L FAN CODE 4120 V CARLSON CODE 4140E H LAST CODE 450D T GRIFFIN 101 STRAUSS AVE INDIAN HEAD MD 20640-5000
1	CDR NSWC INDIAN HEAD DIV LIBRARY CODE 8530 BLDG 299 101 STRAUSS AVE INDIAN HEAD MD 20640
2	US MILITARY ACADEMY MATH SCI CTR OF EXCELLENCE DEPT OF MATHEMATICAL SCI MDN A MAJ D ENGEN R MARCHAND THAYER HALL WEST POINT NY 10996-1786
3	CDR US ARMY YUMA PG STEYP MT AT A A HOOPER STEYP MT EA YUMA AZ 85365-9110
6	CDR NSWC INDIAN HEAD DIV CODE 570D J BOKSER CODE 5710 L EAGLES J FERSUSON CODE 57 C PARIS CODE 5710G S KIM CODE 5710E S JAGO 101 STRAUSS AVE ELY BLDG INDIAN HEAD MD 20640-5035

NO. OF COPIES	ORGANIZATION
1	MICHIGAN STATE UNIVERSITY BRUCE KIM 2120 ENGINEERING BLDG EAST LANSING MI 48824-1226
2	INDUSTRIAL OPERATION CMD AMFIO PM RO W MCKELVIN MAJ BATEMAN ROCK ISLAND IL 61299-6000
3	PROGRAM EXECUTIVE OFFICER TACTICAL AIRCRAFT PROGRAMS PMA 242 1 MAJ KIRBY R242 PMA 242 33 R KEISER (2 CPS) 1421 JEFFERSON DAVIS HWY ARLINGTON VA 22243-1276
1	CDR NAVAL AIR SYSTEMS CMD CODE AIR 471 A NAKAS 1421 JEFFERSON DAVIS HWY ARLINGTON VA 22243-1276
4	ARROW TECH ASSOCIATES INC R WHYTE A HATHAWAY H STEINHOFF 1233 SHELBOURNE RD SUITE D8 SOUTH BURLINGTON VT 05403
3	US ARMY AVIATION CTR DIR OF COMBAT DEVELOPMENT ATZQ CDM C B NELSON ATZQ CDC C T HUNDLEY ATZQ CD G HARRISON FORT RUCKER AL 36362

NO. OF COPIES	ORGANIZATION
	ABERDEEN PROVING GROUND
3	CDR USA ARDEC AMSTA AR FSF T R LIESKE J WHITESIDE J MATTS BLDG 120
1	CDR USA ATEC CSTE CT T J SCHNELL RYAN BLDG
3	CDR USA AMSAA AMXSY EV G CASTLEBURY R MIRABELLE AMXSY EF S MCKEY
60	DIR USARL AMSRL WM I MAY T ROSENBERGER AMSRL WM BA W HORST JR W CIEPELLA AMSRL WM BE M SCHMIDT AMSRL WM BA F BRANDON T BROWN (5 CPS) L BURKE J CONDON B DAVIS T HARKINS (5 CPS) D HEPNER V LEITZKE M HOLLIS A THOMPSON

NO. OF COPIES	ORGANIZATION
	ABERDEEN PROVING GROUND (CONTD)
	AMSRL WM BB B HAUG AMSRL WM BC J GARNER AMSRL WM BD B FORCH AMSRL WM BF J LACETERA P HILL AMSRL WM BR C SHOEMAKER J BORNSTEIN AMSRL WM BA G BROWN B DAVIS T HARKINS D HEPNER A THOMPSON J CONDON W DAMICO F BRANDON AMSRL WM BC P PLOSTINS (4 CPS) G COOPER B GUIDOS J SAHU M BUNDY K SOENCKSEN D LYON A HORST I MAY J BENDER J NEWILL AMSRL WM BC V OSKAY S WILKERSON W DRYSDALE R COATES A MIKHAL J WALL

REPORT DOCUMENTATION PAGE

Form Approved
OMB No. 0704-0188

1. AGENCY USE ONLY *(Leave blank)*	2. REPORT DATE	3. REPORT TYPE AND DATES COVERED
	July 2000	Final, Apr 98 - Mar 99

4. TITLE AND SUBTITLE
Two Projectiles Connected by a Flexible Tether Dropped in the Atmosphere

5. FUNDING NUMBERS
AH80

6. AUTHOR(S)
Geoffrey W. Frost* and Mark F. Costello*

7. PERFORMING ORGANIZATION NAME(S) AND ADDRESS(ES)
Oregon State University
Corvallis, OR 97331

8. PERFORMING ORGANIZATION REPORT NUMBER

9. SPONSORING/MONITORING AGENCY NAMES(S) AND ADDRESS(ES)
U.S. Army Research Laboratory
ATTN: AMSRL-WM-BC
Aberdeen Proving Ground, MD 21005-5066

10.SPONSORING/MONITORING AGENCY REPORT NUMBER
ARL-CR-453

11. SUPPLEMENTARY NOTES
*Oregon State University
Corvallis, OR 97331

12a. DISTRIBUTION/AVAILABILITY STATEMENT
Approved for public release; distribution is unlimited.

12b. DISTRIBUTION CODE

13. ABSTRACT ***(Maximum 200 words)***

This study investigates the atmospheric flight dynamics of a munition system that is released from an aircraft at altitude and drops toward a target on the ground. The munition system consists of two projectiles connected by a tether line. Initially, the two projectiles are rigidly attached. At a specified time, the projectiles separate and subsequently unreel the tether line. After the tether line is fully payed out, the system settles toward a steady state as it approaches the ground. It is shown that while projectile position results converge for a relatively low number of tether line elements, the maximum tether loads require a significantly larger number of elements. For a low follower-to-lead projectile mass ratio, the tether line unreeling process is predominantly due to the follower and lead projectile separation. Conversely, for a high follower-to-lead projectile mass ratio, the tether line tends to billow and subsequently unreel itself, independent of the lead and follower projectile motion.

14. SUBJECT TERMS
aerodynamics, tether, aerial bomb, BDA

15. NUMBER OF PAGES
46

16. PRICE CODE

17. SECURITY CLASSIFICATION OF REPORT	18. SECURITY CLASSIFICATION OF THIS PAGE	19. SECURITY CLASSIFICATION OF ABSTRACT	20. LIMITATION OF ABSTRACT
UNCLASSIFIED	UNCLASSIFIED	UNCLASSIFIED	UL

INTENTIONALLY LEFT BLANK.

USER EVALUATION SHEET/CHANGE OF ADDRESS

This Laboratory undertakes a continuing effort to improve the quality of the reports it publishes. Your comments/answers to the items/questions below will aid us in our efforts.

1. ARL Report Number/Author ARL-CR-453 (Frost) Date of Report July 2000

2. Date Report Received _____

3. Does this report satisfy a need? (Comment on purpose, related project, or other area of interest for which the report will be used.) _____

4. Specifically, how is the report being used? (Information source, design data, procedure, source of ideas, etc.) _____

5. Has the information in this report led to any quantitative savings as far as man-hours or dollars saved, operating costs avoided, or efficiencies achieved, etc? If so, please elaborate. _____

6. General Comments. What do you think should be changed to improve future reports? (Indicate changes to organization, technical content, format, etc.) _____

CURRENT ADDRESS

_____
Organization

_____
Name E-mail Name

_____
Street or P.O. Box No.

_____
City, State, Zip Code

7. If indicating a Change of Address or Address Correction, please provide the Current or Correct address above and the Old or Incorrect address below.

OLD ADDRESS

_____
Organization

_____
Name

_____
Street or P.O. Box No.

_____
City, State, Zip Code

(Remove this sheet, fold as indicated, tape closed, and mail.)
(DO NOT STAPLE)